Plant Physiology Preview. Published on November 8, 2012, as DOI:10.1104/pp.112.203356

Running head: Pleiotropic phenotypes of LIP1

Author to whom all correspondence should be addressed:
László Kozma-Bognár
phone: +36-62-599-717
fax: +36-62-433-434
e-mail: kozmab@brc.hu

Research area: Cell Biology or Development and Hormone Action

The circadian clock-associated small GTPase LIGHT INSENSITIVE PERIOD 1 suppresses light-controlled endoreplication and affects tolerance to salt stress in Arabidopsis[1]

Kata Terecskei[2], Réka Tóth[2], Péter Gyula, Éva Kevei[3], János Bindics, George Coupland, Ferenc Nagy and László Kozma-Bognár[*]

Institute of Plant Biology, Biological Research Centre of the Hungarian Academy of Sciences, H-6726 Szeged, Hungary (K.T., P.G., É.K., J.B., F.N., L.K.-B.)
Department of Plant Developmental Biology, Max Planck Institute for Plant Breeding Research, D-50829, Cologne, Germany (R.T., G.C.)
School of Biological Sciences, University of Edinburgh, EH9 3JR Edinburgh, United Kingdom (F.N.)

Keywords: circadian clock, endoreplication, salt stress, photomorphogenesis, small GTPase

Footnotes:

[1] Work in Szeged, Hungary was supported by grants from the Hungarian Scientific Research Fund to L.K.-B. (OTKA- 106361) and to F.N. (OTKA-81399) and by the New Hungary Development Plan project (TÁMOP-4.2.2-08/1-2008-0007) to F.N. Work in Cologne, Germany was supported by EC-funded Agro-nomics, the DFG DIP programme and Chemical Genomics Centre of the Max Planck. Work in Edinburgh, UK was supported by a Research Chair Award to F.N. from the Scottish Universities Life Science Alliance (SULSA). L.K.-B. was supported by the János Bólyai Research Scholarship from the Hungarian Academy of Sciences and by the New Hungary Development Plan project (TÁMOP- 4.2.2/B-10/1-2010-0012).

[2] These authors contributed equally to this work

[3] Present address: Cluster of Excellence: Cellular Stress Responses in Aging-Associated Diseases (CECAD) Cologne at the Institute for Genetics, University of Cologne, D-50674 Cologne, Germany

* Corresponding author; e-mail: kozmab@brc.hu; fax: +36-62-433-434

ABSTRACT

Circadian clocks are biochemical timers regulating many physiological and molecular processes according to the day/night cycles. The small GTPase LIGHT INSENSITIVE PERIOD 1 (LIP1) is a circadian clock- associated protein that regulates light input to the clock. In the absence of LIP1, the effect of light on free-running period length is much reduced. Here we show that in addition to suppressing red and blue light-mediated photomorphogenesis, LIP1 is also required for light-controlled inhibition of endoreplication and tolerance to salt stress. We demonstrate that in the processes of endoreplication and photomorphogenesis LIP1 acts downstream of the red and blue light photoreceptors phytochrome B and cryptochromes. Manipulation of the subcellular distribution of LIP1 revealed that the circadian function of LIP1 requires nuclear localization of the protein. Our data collectively suggest that LIP1 influences several signaling cascades and that its role in the entrainment of the circadian clock is independent from the other pleiotropic effects. Since these functions of LIP1 are important for the early stages of development or under conditions normally experienced by germinating seedlings, we suggest that LIP1 is a regulator of seedling establishment.

INTRODUCTION

Optimal growth and development of plants are mediated by various signaling pathways, which enable plants to modulate their molecular and physiological reactions in response to changes of the environment. Light, the sole energy source is the most important environmental factor for plants. To monitor changes in ambient light conditions, plants evolved several families of photoreceptors covering the visible and the UV-A/B region of the spectrum (Franklin and Quail, 2010; Chaves et al., 2011; Rizzini et al., 2011). The red/far-red light absorbing phytochromes (PhyA-E) and the blue light absorbing cryptochromes (CRY1 and 2) are considered to mediate the majority of physiological and developmental responses to visible light.

Besides regulating photomorphogenesis, these photoreceptors also play an essential role in entraining/synchronizing the circadian clock to the daily light/dark cycles (Devlin and Kay, 2000). This process is important, since the circadian clock is not a linear signaling system, but rather modulates and co-ordinates signaling pathways and physiological processes through the day/night cycles (Covington et al., 2008). Synchronization of the clock with the objective time enables organisms to anticipate predictable changes of environmental parameters or the expected onset of stresses, which in turn may confer selective advantages (Dodd et al., 2005; Legnaioli et al., 2009).

The clock is a biochemical mechanism relying on the mutual feed-forward/feed-back regulation of the so-called clock genes and proteins. The rhythm-generating module (also called central oscillator) of the Arabidopsis clock consists of at least three interconnected genetic circuits (Pruneda-Paz and Kay, 2010; Huang et al., 2012). In addition to the basic transcriptional regulation, post-translational modifications, regulated proteolysis or controlled nucleo-cytosolic transport of clock proteins also play important roles in the clock mechanism (Mas, 2008; Wang et al., 2010). The central clockwork generates the primary oscillation in the expression of clock components with a period of about 24 h. The oscillation is then relayed to the expression of downstream components. In Arabidopsis, 15-25% of the transcriptome is regulated rhythmically. Circadian regulation is clearly over-represented among the genes that are implicated in light, hormonal or stress signaling, suggesting a molecular basis for the temporal modulation of these pathways (Covington et al., 2008).

Among these pathways, high salinity stress represents ionic (high [Na+]) and osmotic stress and the responses of plant cells consist of several consecutive as well as parallel steps (Yamaguchi-Shinozaki and Shinozaki, 2006). The early responses involve increase in Ca^{2+} flux leading to SOS protein mediated changes in ion homeostasis. Ca^{2+} flux and other secondary messengers such as phospholipids and reactive oxygen species (ROS) activate kinase signaling cascades triggering the transcription of rapid stress-inducible genes. These responses can be ABA-dependent and -independent, and both of these are linked to the circadian clock in several ways (Sanchez et al., 2011). For example, ABA induces *TOC1* expression at midday, which leads to circadian control of the ABA-related gene *ABAR*/*GUN5* (Legnaioli et al., 2009). This feedback mechanism ensures the correct timing and sensitivity of ABA signalling and stomata opening. As a consequence, TOC1 overexpression results in reduced ABA-mediated drought tolerance due to impaired stomata opening. Furthermore, ABA precursors, biosynthesis genes and several ABA-responsive genes are diurnally expressed and show altered transcription in circadian clock mutants, like the *prr9,7,5* triple mutant or the CCA1 over-expressor (Fukushima et al., 2009). As for ABA-independent stress pathways, upregulation of the DREB1/CBF regulon was described in the *prr9,7,5* triple mutant, which displayed enhanced salt, drought and cold tolerance (Nakamichi et al., 2009), whereas the same regulon was downregulated in the *lhy cca1* double mutant, which exhibited reduced cold and salt tolerance (Kant et al., 2008; Dong et al., 2011). Hours after the onset of stress, a slower adaptation process starts, leading to stomata opening and accumulation of osmolytes, secondary metabolites and free radical scavengers, which protect the plant from stress damage.

Adaptation to the changing environment also requires plasticity of the developmental program both at the organism and the cellular levels. In fact, even core biochemical processes, such as the cell cycle, can be modulated by environmental factors. For example, in Arabidopsis, hypocotyl cells undergo several endocycles in the dark, but the last cycle is inhibited in the light (Gendreau et al., 1998). During this process, DNA replication is correctly initiated and terminated, but is not followed by the separation of the chromosomes and cytokinesis (De Veylder et al., 2011). As a result, the cellular DNA is exactly doubled after each endocycle. Very recently, the light-regulated transcription of

an atypical E2F transcription factor, DP-E2F-LIKE1 (DEL1), was proposed as the key mediator of light regulation of endoreplication (Berckmans et al., 2011). *DEL1* transcription is positively or negatively regulated by the typical E2Fb or E2Fc transcription factor, respectively (Berckmans et al., 2011). E2Fb protein degradation is facilitated by the E3 ubiquitin ligase COP1, resulting in low expression level of *DEL1* in the dark. In the light, however, COP1 is inactivated by various photoreceptor-mediated mechanisms, thus E2Fb protein levels rise, causing an increase in *DEL1* transcription. DEL1 directly represses the transcription of *FZR1/CCS52A2*, which is an activator of the anaphase promoting complex (APC) (Lammens et al., 2008). APC is responsible for the degradation of mitotic cyclins leading to the inactivation of cyclin-cyclin dependent kinase (CYC/CDK) complexes and the onset of endoreplication (De Veylder et al., 2011). Since DEL1 attenuates APC function mainly in the light, endoreplication is inhibited under these conditions.

Previously, we identified the small GTPase LIGHT INSENSITIVE PERIOD 1 (LIP1) as a circadian clock-associated factor in Arabidopsis (Kevei et al., 2007). Loss of LIP1 function in the *lip1-1* mutant severely reduced the effect of light on the shortening of free-running period length. Essentially, this resulted in a short period phenotype of *CAB2:LUC* expression at low fluences of red and blue light. In the present work we provide physiological and molecular data demonstrating that (i) LIP1 is involved in mediating PhyB-controlled photomorphogenesis, (ii) LIP1 is a component of the PhyB-controlled red and CRY-controlled blue light signaling cascade inhibiting endoreplication, (iii) LIP1 is required for normal development of pavement cells in young seedlings, and (iv) LIP1 function is needed for salt tolerance. Moreover, by manipulating the subcellular localization of LIP1, we show that the circadian function of LIP1 can be separated from its other functions not only at the physiological, but also at the cellular level.

RESULTS

Loss of function of LIP1 protein causes altered cell shape

Microscopic analysis of young *lip1-1* and *lip1-2* mutant seedlings (Kevei et al., 2007) revealed defects in cell development. In wild-type Arabidopsis plants pavement cells

have a characteristic jigsaw puzzle shape with lobes, whereas both in *lip1-1* and *lip1-2* mutants the cell shape was more rounded and much less complex (Fig.1A). The shape factor, describing the roundness of the cells, indicated a significant difference between *lip1* mutants and the corresponding wild types (Fig.1B).

Additionally, we observed that *lip1-2* mutants showed characteristic, upward curling cotyledons (Fig.1C). This morphological change is the result of the non-continuous layer of pavement and leaf blade cells that never occurs in wild-type plants (Fig.1C-D). This phenomenon is most likely caused by cell death, since the shapes of the stomata guard cells and pavement cells were still visible in the patches lacking epidermal cells (Fig.1D). In fact, the remaining pavement cells form islands on the top of mesophyll cells (Fig.S1). Unlike *lip1-2* seedlings (Fig.1C), *lip1-1* plants displayed a continuous layer of pavement cells in the cotyledon, indicating ecotype-specific differences, as both mutant alleles are loss-of-function alleles (Kevei et al., 2007). In addition, our data suggest that the cell shape and discontinuous pavement cell layer phenotypes are developmentally regulated, because pavement cells in the first true leaves of *lip1-1* and *lip1-2* mutants had wild-type morphology (Fig.1E). These observations suggest that LIP1 has a more pronounced function during the early developmental stages of the plant life cycle.

LIP1 affects ploidy levels in seedling stage

The alteration of cell morphology is frequently linked with changes in nuclear DNA content (Guimil and Dunand, 2007). Therefore, we analyzed ploidy patterns in the cotyledons of *lip1* mutants by flow cytometry, and found that the proportion of nuclei having high DNA content was significantly increased in the mutants (Fig.2A-B). In particular, the ratio of 16C nuclei was elevated and, unlike in wild type, even 32C nuclei were detectable in *lip1-2* cotyledons (Fig.2B). Changes in ploidy levels are often associated with altered cell size or cell number. These parameters were determined for the pavement and the palisade mesophyll cells in *lip1-1* and wild type cotyledons (Table 1). Interestingly, elevated ploidy levels in *lip1-1* were accompanied by a reduction in the size of these cell types, but the total number of cells was not affected suggesting that LIP1 does not affect the mitotic cell cycle. In agreement with the reduced cell size, the area of *lip1-1* cotyledons was significantly smaller than that of the wild type (Table 1).

To test if nuclear DNA content is affected by LIP1 in other parts of the seedlings, samples of hypocotyls or entire seedlings were used in the assay (Fig.2C-D). Ploidy patterns in isolated hypocotyl of *lip1-2* mutant showed the same tendency as in the cotyledons, demonstrating that in seedling stage the effect of LIP1 on endoreplication is not organ-specific. In contrast, ploidy patterns in the matured first leaves of *lip1-2* and wild-type plants were not significantly different (Fig.2E), suggesting that LIP1 suppresses ploidy levels in a developmentally regulated manner.

Light-dependent inhibition of endoreplication by LIP1

Four cycles of endoreplication could occur in dark-grown Arabidopsis seedlings, whereas the fourth cycle is inhibited in light (Gendreau et al., 1998). Since LIP1 is involved in the light regulation of the circadian clock and photomorphogenic processes (Kevei et al., 2007), we analyzed ploidy patterns in *lip1* mutants grown under different light conditions. Elevated ploidy level was detected in *lip1* seedlings grown under light-dark cycles (Fig.3 C-D), and the DNA content increased further when plants were grown in continuous white light (Fig.3E-F). However, ploidy levels were identical in etiolated *lip1* and wild-type seedlings (Fig.3A-B), demonstrating that LIP1 suppresses endoreplication in a light-dependent manner. We also characterized pavement and palisade mesophyll cells in the cotyledons of etiolated C24 and *lip1-1* seedlings. In contrast to light-grown plants (Fig.1A and Table 1), the shape, number and size of these cells types were not significantly different in the wild-type and the mutant seedlings grown in the dark (Fig.S2 and Table 2). These results demonstrate that the cell morphology phenotype of *lip1* mutants is light dependent.

In red light, the light-induced inhibition of endoreplication depends on the photoreceptor Phytochrome B (PhyB), as dark or red-light grown *phyB* mutants have identical, high ploidy levels (Gendreau et al., 1998). To test the epistatic relation between LIP1 and PhyB in controlling red light-dependent endoreplication, ploidy levels of *lip1-2*, *phyB-9* single and *lip1-2 phyB-9* double mutants were compared. In continuous red light (cR), both *lip1-2* and *phyB-9* mutants showed similarly increased ratios of 16C and 32C nuclei (Fig.4B). Importantly, the *lip1-2 phyB-9* double mutant did not display additive phenotype but phenocopied the *phyB-9* single mutant in cR (Fig.S3). The DNA content

of these mutants grown in darkness displayed patterns like wild-type seedlings, confirming the light-specific effect of the mutations (Fig.4A).

Next, we examined whether LIP1 affects endoreplication in other light conditions, such as in continuous blue (cB) or far-red light (cFR). Ploidy levels of *lip1-2* mutant showed significant increase in cB (Fig.4D, Fig.S4), but it was indistinguishable from the wild-type in cFR (Fig.4E). To place LIP1 in the light signaling pathway, the mutation in *LIP1* gene was combined with the mutations in genes coding for the blue light absorbing CRY1 and CRY2 or far-red sensing PhyA receptors and seedlings were tested in cB or cFR. In cB light, the ploidy pattern of the *lip1-2 cry1 cry2* triple mutant was most similar to that of the *cry1 cry2* double mutant (Fig.4D, Fig.S4) suggesting that LIP1 is epistatic to the CRY photoreceptors. In cFR light, the *lip1-2 phyA-211* double mutant phenocopied the *phyA-211* single mutant (Fig.4E), further supporting the previous finding that LIP1 is not involved in far-red light specific control of endoreplication. In summary, these results indicate that LIP1 plays an important role in integrating red and blue light signals to inhibit endoreplication. Furthermore, LIP1 is likely to function downstream of PhyB and CRY photoreceptors.

The light-regulated transcription of the atypical E2F transcription factor DEL1 was suggested to play a key role in the light regulation of endoreplication (Berckmans et al., 2011). To test the involvement of LIP1 and PhyB in light-regulated transcription of DEL1, we determined levels of *DEL1* mRNA in the wild type and in *lip1-2, phyB-9* and *lip1-2 phyB-9* mutants grown in darkness or cR. In wild-type plants *DEL1* mRNA levels were higher in the light than in darkness (Fig.4F), in agreement with previous results (Berckmans et al., 2011). Interestingly, the red light-induced upregulation of *DEL1* expression was clearly detectable in all genotypes, including *phyB-9* single mutant. Furthermore *DEL1* mRNA levels in any of the tested mutants showed no significant differences compared to the wild type (Fig.4F). These data suggest that in red light, LIP1 and PhyB do not inhibit endoreplication through the transcriptional control of *DEL1*.

Function of LIP1 in controlling photomorphogenesis depends on PhyB and CRY1 and 2, but is independent of PhyA

It had been demonstrated that *lip1-1* mutants show elevated photomorphogenic responses (short hypocotyls) to red and blue, but not to far-red light (Kevei et al., 2007). In order to place the action of LIP1 in light signaling pathways mediated by phytochrome and cryptochrome photoreceptors, we characterized the responsiveness of *lip1-2 phyB-9*, *lip1-2 phyA-211* and *lip1-2 cry1 cry2* multiple mutants to R, FR and B light, respectively. In cR the *lip1-2* mutant showed significantly shorter hypocotyls than the wild type; however, the *lip1-2 phyB-9* double mutant produced hypocotyls much longer than the wild type, and was very similar to that of the *phyB-9* single mutant (Fig.5A, Fig.S5A). In cB the *lip1-2* mutant displayed less pronounced, but significant hypersensitivity compared to the wild-type, but *lip1-2 cry1 cry2* produced long hypocotyls similarly to the *cry1 cry2* double (Fig.5B, Fig.S5B). In continuous FR *lip1-2* phenocopied wild-type plants, and *lip1-2 phyA-211* double mutant showed hypocotyl lengths identical to that of the *phyA-211* mutant (Fig.5C, Fig.S5C). These data verify that LIP1 does not affect PhyA-dependent far-red light signaling. The photomorphogenic phenotype of *lip1* mutants in red light is mainly due to the perturbation of PhyB-mediated signaling, whereas the *lip1* phenotype in blue light depends on the CRY photoreceptors. Absolute hypocotyl length data are provided in Figure S6.

lip1 mutants are hypersensitive to salt stress

In order to obtain additional information on the function of LIP1 we determined the responsiveness of *lip1* mutants to different abiotic stress conditions. We found that *lip1* mutants grown under 12:12 LD cycles displayed an increased sensitivity to salt (NaCl) stress (Fig.S7 and Fig.5D-E). Wild-type plants could tolerate 100 mM NaCl, but the growth and development of mutant *lip1* seedlings were greatly impaired under these conditions (Fig.S7). *lip1-1* mutants were slightly less sensitive to NaCl than *lip1-2* mutants, which is probably due to ecotype-specific differences, as wild-type C24 seedlings appeared to be more tolerant than Columbia-0 (Fig.S7). In addition to poor growth and development, the germination rate of *lip1-2* seedlings was also significantly reduced under salt stress conditions as compared to the wild type (Fig.5E). To test if light conditions modulate this stress response, germination rate was also analyzed in dark-grown plants. Under these conditions *lip1-2* mutants were again more sensitive than wild-

type plants (Fig.5E), indicating that the salt stress phenotype is not caused by other light-dependent defects of *lip1* mutants (e.g. ploidy levels). Besides inhibiting germination, high NaCl concentration also attenuates root growth; therefore we determined this response of *lip1* mutants grown on different concentrations of NaCl. Figure 5F illustrates that the relative inhibition of root growth is significantly stronger in the *lip1* mutants than in the wild type. These data demonstrate that LIP1 is required for maximum tolerance to salt stress.

High salinity represents osmotic and ionic stress for plants. Osmotic stress leads to the induction of osmoprotectant genes like *RD29A*, *RD29B* or *RAB18*, whereas ionic stress (increase in the cellular [Na+]) induces the transcription of *SOS2*, an activator of the Na+/H+ transporter SOS1. To test if LIP1 participates in any of these processes, one-week-old wild-type and *lip1-2* plants were transferred to media containing 200 mM NaCl. Salt-induced expression of *RD29A*, *RD29B*, *RAB18* and *SOS2* genes was monitored by qRT-PCR. Figure S8 demonstrates that there were no significant differences in the kinetics or the level of induction of these genes. These results indicate that LIP1 plays a minor role, if any, in sensing salt stress signals and the transcriptional activation of the salt stress related genes tested. However, an effect of LIP1 on the post-translational modification, turnover or subcellular localization of these components cannot be excluded.

Subcellular localization of LIP1

We showed previously that the YFP-LIP1 fusion protein is detectable both in the cytosol and in the nucleus, and that this distribution pattern is not significantly affected by light conditions or the circadian clock (Kevei et al., 2007). In order to test if any of the pleiotropic functions of LIP1 described above requires specific subcellular localization, we generated transgenic *lip1* plants expressing the LIP1-YFP fusion protein with or without a nuclear localization signal (NLS) or a nuclear export signal (NES) (Fig.S9A) Transgenic lines with comparable expression levels were selected (Fig.S9B) and localization of the different LIP1 fusion proteins was analyzed by fluorescent microscopy. As expected, YFP-LIP1 was detectable both in the cytoplasm and in the

nuclei, whereas YFP-LIP1-NLS and YFP-LIP1-NES were clearly restricted to the nucleus and the cytoplasm, respectively (Fig.S9C).

Nuclear localization of LIP1 is essential for the circadian function of the protein

Complementation of the ploidy, salt stress, photomorphogenic and circadian phenotypes of the *lip1* mutants was tested in the selected transgenic lines. Figure 6A demonstrates that the expression of YFP-LIP1, YFP-LIP1-NLS or YFP-LIP1-NES in the *lip1* mutant background restored ploidy levels to wild-type level, best illustrated by the ratio of nuclei having 16C or 32C DNA content. In addition to ploidy levels, the characteristic jigsaw shape of cotyledon pavement cells was also restored in all complemented lines (Fig.S10). Furthermore, *lip1-2* plants expressing either of the LIP1 fusion proteins were able to tolerate 100 mM NaCl and develop similarly to wild-type plants (Fig.6B). Hypocotyl lengths of either of the complemented lines grown in red, blue or far-red light were also indistinguishable from that of the wild type (Fig.7A-C). These data suggest that compartmentalization of LIP1 is not sufficient to abrogate LIP1 function for mediating these responses. However, the compartmentalization of LIP1 distinguishes its function concerning circadian rhythmicity (Figure 7D-F and Table 3). Expression of YFP-LIP1 or YFP-LIP1-NLS restored wild-type circadian rhythms, whereas YFP-LIP1-NES expressing transgenic *lip1-2* seedlings displayed rhythms very similar to that of *lip1-2*. Period estimates quantitatively demonstrated full complementation or the complete lack of complementation as indicated (Table 3). We conclude that for the regulation of the circadian clock a significant portion of LIP1 needs to be present in the nucleus. These observations suggest that the function of LIP1 in the circadian clock can be separated from its role in the control of cell development, endoreplication, stress tolerance and photomorphogenesis.

DISCUSSION

The *lip1-1* mutant was identified in a genetic screen designed to isolate novel circadian clock mutants in Arabidopsis (Kevei et al., 2006; Kevei et al., 2007). The *lip1-1* mutation shortened the free-running period of *CAB2:LUC* in low intensity red light and the mutant showed hypersensitive photomorphogenic responses in red and blue light. In this paper

we demonstrate that the *lip1-1* and *lip1-2* mutants display additional pleiotropic phenotypes and that LIP1 also plays important roles in the light-controlled inhibition of endoreplication and providing tolerance to salt stress.

It has been shown that far-red and red light perceived by the PhyA and PhyB photoreceptors inhibits the last round of endocycles in hypocotyl cells in Arabidopsis, whereas the receptor mediating the effect of blue light was not identified unequivocally (Gendreau et al., 1998). *lip1* mutants showed higher ploidy levels in white, red and blue light, but not in darkness or in far-red light (Fig.3 and 4). This indicates that the ploidy phenotype of *lip1* mutants arose from the impaired red and blue light control of endoreplication. In fact, genetic analysis of red and blue light controlled ploidy patterns demonstrated that *PHYB* and *CRY1* and *2* are epistatic to *LIP1* (Fig4.). This suggests that LIP1 functions as a component of the PhyB- and CRY1 and 2-mediated light signaling pathways leading to the inhibition of endoreplication. Apart from the receptors, the atypical E2F transcription factor DEL1 was recently shown to mediate light-dependent endoreplication (Berckmans et al., 2011). In particular, transcription of *DEL1* is light-induced and negatively correlated with ploidy levels, and ectopically expressed *DEL1* uncouples the regulation of endoreplication from light signals (Berckmans et al., 2011). Here we show that the level of *DEL1* mRNA in *phyB-9, lip1-2* and *lip1-2 phyB-9* plants was not significantly different from that in wild-type plants (Fig.3). These data demonstrate that red light-induced inhibition of endoreplication by PhyB and LIP1 define a pathway independent of the transcriptional regulation of *DEL1*.

Changes in ploidy levels are often accompanied by altered shape or size of the cells. In fact, we showed that pavement cells in the cotyledons of *lip1* mutants are significantly smaller and more rounded (or less lobed) compared to those in wild-type plants. The cell morphology phenotype of *lip1* mutants appears to closely correlate with ploidy changes since both phenotypes are developmentally regulated and light dependent in the same manner. In wild-type plants, cells with higher ploidy levels are usually larger, but there are several examples from mutants where increased ploidy levels are not accompanied by growth promotion, or the size of particular cells is enlarged without significant increase of DNA content (De Veylder et al., 2011). Moreover, strong over-expression of Kip-

related protein 2 (KRP2), an inhibitor of CDKA;1, resulted in lower ploidy levels, but yet larger pavement cells (Verkest et al., 2005). *lip1* mutants represent a novel class of exceptions, where cells with higher ploidy levels are apparently smaller in size. These observations collectively suggest that cellular DNA content does not control cell expansion directly, but probably sets the range or capacity of future cell growth, which is influenced by the co-action of several additional factors.

In order to shed light on the molecular background of salt sensitivity of *lip1* mutants, the function of the canonical osmotic and ionic stress signaling pathway was probed. As in the *lip1* mutants salt stress induced the transcription of both ABA-dependent and independent stress related genes normally (Fig.S8), we suggest that stress perception, signaling cascade and transcriptional activation of the multiple pathways were not impaired by the lack of LIP1 function. Rather, LIP1 could affect one of the late stress-induced processes at the cellular level. A likely target of LIP1 action could be the regulation of ROS production, as small GTPases are involved in this process in animals, yeast and plants as well (Finkel, 2006). A ROP-type small GTPase OsRAC1 in rice was shown to directly interact with NADPH oxidase and hence modulate ROS production (Wong et al., 2007). OsRAC1 and its Arabidopsis homolog ROP2 exhibit altered responses to biotic and abiotic stresses accompanied with apoptosis-like cell death (Ono et al., 2001; Park et al., 2004). In addition to stress sensitivity, *lip1-2* mutant also shows cell death symptoms, however this is restricted to the cotyledon epidermis cells (Fig. 1 and S1), unlike the necrotic lesions on leaves observed in dominant negative RAC1. Furthermore, the ROS-linked small GTPases are localized mostly in the plasma membrane, which is in contrast with the nucleo-cytoplasmic localization of LIP1 (Fig.S9) and the complementation of stress hypersensitivity by the nuclear targeted LIP1 protein (Fig.5). Despite these differences it is tempting to speculate that alterations in cell morphology and cell death in the epidermis could affect the “barrier” function of this cell layer in the *lip1* mutants, so that the excess of salt taken up cannot be compensated by the otherwise intact salt signaling and response system. However, dark-grown *lip1* mutants without apparent cell morphology phenotypes were also hypersensitive to salt stress, therefore we conclude that salt sensitivity of *lip1* mutants is not caused by abnormally shaped (or missing) pavement cells.

The shortening of circadian period by *lip1* mutantion is clearly detectable in etiolated plants (Kevei et al., 2007), where ploidy levels of *lip1* mutants do not differ from that of the wild type. On the other hand, the salt sensitivity, photomorphogenic and ploidy phenotypes of *lip1* mutants could be detected under conditions, where the mutants did not show circadian defects (i.e. high fluence rate of red or white light) (Kevei et al., 2007). These facts strongly suggest that (i) the circadian function of LIP1 is independent from its other functions, and (ii) the altered function of the clock in the *lip1* mutants is not the cause of the stress, ploidy or hypocotyl phenotypes. This conclusion is further corroborated by the results of the complementation experiments. The circadian phenotype was complemented by YFP-LIP1 and YFP-LIP1-NLS, but not by YFP-LIP1-NES, indicating that LIP1 must accumulate to a critical level in the nucleus in order to regulate the clock. The full complementation of the circadian phenotype also suggests that LIP1 does not affect clock-related cytosolic processes, although its role in mediating nucleo-cytoplasmic partitioning of clock components cannot be excluded. Interestingly, all the other phenotypes were equally complemented by YFP-LIP1, YFP-LIP1-NLS or YFP-LIP1-NES. It must be noted, however, that although addition of NLS or NES motifs dramatically alters the subcellular localization of LIP1, by no means does it completely restrict the protein to the nucleus or the cytoplasm. Particularly, the NES motif does not prevent nuclear import, but facilitates nuclear export, thereby reducing the average time spent by the tagged LIP1 protein in the nucleus. It follows that the very small amount of YFP-LIP1-NES present in the nucleus could be sufficient to mediate certain functions (e.g. controlling endoreplication). This amount is clearly insufficient for restoring circadian functions, demonstrating the great demand of the clock for nuclear LIP1. However, it would be premature to designate certain cellular compartments as locations of LIP1 protein fractions affecting salt stress, photomorphogenesis or endoreplication.

In plants LIP1 is the founder of a novel and therefore not well-characterized subclass of small GTPases, and it is the only small GTPase which has been functionally linked to the regulation of the circadian clock (Kevei et al., 2007). Interestingly, some members of the ROP, RAB subfamilies were shown to modulate responses similar to LIP1. For example,

ROP GTPases (ROP2, 4 and 6) were reported to control the shape of pavement cells via the assembly and organization of cortical microfilament and microtubule networks (Fu et al., 2005; Fu et al., 2009). ARA6 is a RAB-type GTPase implicated in vesicular trafficking between endosomes and the plasma membrane and, similarly to LIP1, it is required for tolerance to high salinity (Ebine et al., 2011). More recently, it has been suggested that the activity of the ROP8 GTPase is regulated by phytochromes, which probably accounts for light-dependent control of root elongation by ROP8 (Shin et al., 2010). However, further studies are required to elucidate the molecular mechanisms by which functions of these small GTPases are integrated at the cellular level.

Our results indicate that LIP1 facilitates germination under suboptimal conditions, entrains the circadian clock in plants germinating/elongating in the soil at limited light intensities and controls normal morphology of the emerged young seedlings; therefore, we suggest that LIP1 is an important modulator of seedling establishment. However, it is unlikely that all functions of LIP1 are limited to the seedling stage, since LIP1 is clearly expressed in most tissues of adult plants. The lack of cell shape and ploidy phenotypes in adult *lip1* mutant plants can be explained by the presence of developmentally regulated proteins functionally redundant to LIP1 or by the availability of different interacting partners at different developmental stages. Identification of conformation-specific interacting proteins, which regulate the activity of LIP1 or act as effectors downstream to LIP1, will be essential for delineating the molecular function of this small GTPase in diverse signaling cascades.

MATERIALS AND METHODS

Plant materials and growth conditions

Arabidopsis thaliana ecotypes of C24 and Columbia-0 (Col-0) were used as wild-type plants. *lip1-1* and *lip1-2* alleles are in the C24 and Col-0 backgrounds, respectively (Kevei et al., 2007). The *phyA-211*, *phyB-9*, and the *cry1-304 cry2-1* mutants (all in the Col ecotype) have been described (Reed et al., 1993; Reed and Chory, 1994; Mockler et al., 1999). The *cry1-304 cry2-1* double mutant is referred to as *cry1 cry2* in the text. Surface-sterilized seeds were stratified at 4^{o}C for 3 days and grown in 12 h white light /

12 h dark (12:12 LD) photocycles at 22^{o}C for 7 days, unless indicated otherwise. Seedlings for ploidy level measurements, cell morphology determinations and *DEL1* qRT-PCR assays were grown on half-strength Murashige and Skoog (MS) media supplemented with 1% (w/v) sucrose. Plants for luminescence detection, salt tolerance tests and the investigation of salt-induced gene expression were grown on MS media supplemented with 3% (w/v) sucrose. For hypocotyl elongation tests, seedlings were sown on wet filter paper. Special growth conditions are described below or in the corresponding figure legends.

Gene constructs and transgenic plants

Transgenic *lip1-1* plants expressing the YFP-LIP1 fusion protein under the control of the CaMV 35S promoter, and the modified pPCV812 binary vectors containing the 35S promoter and DNA fragments coding for YFP and NLS or NES motifs have been described (Kevei et al., 2007; Palagyi et al., 2010). To create 35S:YFP-LIP1-NLS/NES constructs, the LIP1 cDNA fragment was inserted in the modified pPCV812 vectors, between the YFP and NLS/NES fragments. The constructs were transformed in *lip1-1* and *lip1-2* mutant plants expressing the *CAB2:LUC* marker (Clough and Bent, 1998). Transformants were selected on Murashige and Skoog medium supplemented with 15 µg mL^{-1} of hygromycin. 10 to 15 independent transformants for each construct were self-fertilised, and individuals of the homozygous T3 progenies were used for experiments.

Scanning electron microscopy

Scanning electron microscopy was carried out using a Zeiss Supra 40VP (Carl Zeiss SMT AG) equipped with a field emission gun (FEG) as electron source, secondary electron detector for imaging and combined with Emitech K1250X (Quorum Emitech) transfer system. The biological samples were prepared with cryogenic preparation method. Fresh tissue parts were mounted onto the probe holder using Tissue-Tec (O.C.T. Compound) as glue, and gold/palladium was used for sputter coating.

Differential interference microscopy (DIC) and calculation of shape factor

7 day old seedlings were cleared overnight in a solution composed of 160 g of chloral hydrate (Sigma-Aldrich), 100 mL of water, and 50 mL of glycerol. After clearing, cotyledons were mounted with a cover slip and pavement cells visualized with a Leica DMRB microscope equipped with DIC optics (Leica). Images were captured on a Leica DFC 490 camera using the Leica Application Suite 2.5.0 software. Cell area and perimeter of matured pavement cells were measured with ImageJ software and shape factor calculated as 4π area/perimeter^2. Statistical significance was assessed with t-test calculated with SigmaStat 3.5 software.

Confocal laser scanning microscopy

Cotyledons of 7-day-old seedlings were mounted on glass slides and fluorescence was detected with confocal laser-scanning microscopy Leica TCS SP2 AOBS CLSM system equipped with 40× and 63× lenses, an argon-krypton laser and a 405 nm diode laser (Leica).

Ploidy measurement with flow cytometry

Plant material was cut with razor blade, stained with CyStain UV precise P DNA staining kit (Partec) then filtered though 50 μm mesh. Ploidy level of samples was measured with Ploidy Analyser PA-1 (Partec) and analyzed with FloMax 2.52 software (Partec). Statistical significance was calculated with SigmaStat 3.5 software.

Physiological assays

For luminescence detection, seedlings were grown in 12:12 LD cycles for 7 days and transferred to continuous red light (SnapLite, Quantum Devices) at 5 μmol m^{-2} s^{-1} fluence rate. Luminescence was monitored for 4 days using the TopCount NXT luminometer (Perkin Elmer) as described (Kevei et al., 2007). Counts were normalized to the average of counts collected during the entire measurement and were plotted as normalized luminescence.

For salt tolerance assays, seedlings were germinated in 12:12 LD cycles for 14 days on media containing NaCl at different concentrations. To test the effect of high salinity on germination rate, seeds were sown on media with or without 200 mM NaCl. The plates

were transferred to 12:12 LD or to constant darkness. Germinated seeds with clearly visible radicles were counted daily for 5 days. To assess germination on subsequent days in darkness, separate plates were moved to light on each day and germinating seedlings were counted. For root length measurements, seedlings were grown in 12:12 LD cycles for 7 days on salt-free media and transferred to media supplemented with different concentration of NaCl. The plates were set to vertical position and length of roots was measured 7 days after the transfer. Values were normalized to the length of roots of non-treated plants.

Hypocotyl lengths were measured essentially as described (Palagyi et al., 2010).

Analysis of gene expression

To determine *DEL1* mRNA levels, plants were grown in continuous red light (40 μmol m^{-2} s^{-1}) or in darkness for 7 days before samples were harvested. To measure *RD29A*, *RD29B*, *RAB18* and *SOS2* mRNA levels, plants were grown in 12:12 LD cycles for 7 days and transferred to media with or without 200 mM NaCl and samples were harvested 1, 3, 6, 9 and 12h after the transfer. Isolation of total RNA, cDNA synthesis and qRT-PCR were carried out as described (Palagyi et al., 2010). Specific mRNA levels were normalized to *TUBULIN2/3* mRNA levels in each sample. Sequences of primers used for qRT-PCR assays are shown in Table S1. Averages of results from three independent experiments are shown; error bars represent standard error values.

ACKNOWLEDGEMENTS

We thank the Central Microscopy Service (CeMic) of MPIPZ in Cologne for help with DIC and SEM microscopy. We are grateful to Gabriella Veres for excellent technical assistance and Erzsebet Fejes for critical reading of the manuscript.

LITERATURE CITED

Berckmans B, Lammens T, Van Den Daele H, Magyar Z, Bogre L, De Veylder L (2011) Light-dependent regulation of DEL1 is determined by the antagonistic action of E2Fb and E2Fc. Plant Physiol **157:** 1440-1451

Chaves I, Pokorny R, Byrdin M, Hoang N, Ritz T, Brettel K, Essen LO, van der Horst GT, Batschauer A, Ahmad M (2011) The cryptochromes: blue light photoreceptors in plants and animals. Annu Rev Plant Biol **62:** 335-364

Clough SJ, Bent AF (1998) Floral dip: a simplified method for Agrobacterium-mediated transformation of Arabidopsis thaliana. Plant Journal **16:** 735-743

Covington MF, Maloof JN, Straume M, Kay SA, Harmer SL (2008) Global transcriptome analysis reveals circadian regulation of key pathways in plant growth and development. Genome Biol **9:** R130

De Veylder L, Larkin JC, Schnittger A (2011) Molecular control and function of endoreplication in development and physiology. Trends in Plant Science **16:** 624-634

Devlin PF, Kay SA (2000) Cryptochromes are required for phytochrome signaling to the circadian clock but not for rhythmicity. Plant Cell **12:** 2499-2510

Dodd AN, Salathia N, Hall A, Kevei E, Toth R, Nagy F, Hibberd JM, Millar AJ, Webb AA (2005) Plant circadian clocks increase photosynthesis, growth, survival, and competitive advantage. Science **309:** 630-633

Dong MA, Farre EM, Thomashow MF (2011) Circadian clock-associated 1 and late elongated hypocotyl regulate expression of the C-repeat binding factor (CBF) pathway in Arabidopsis. Proc Natl Acad Sci U S A **108:** 7241-7246

Ebine K, Fujimoto M, Okatani Y, Nishiyama T, Goh T, Ito E, Dainobu T, Nishitani A, Uemura T, Sato MH, Thordal-Christensen H, Tsutsumi N, Nakano A, Ueda T (2011) A membrane trafficking pathway regulated by the plant-specific RAB GTPase ARA6. Nat Cell Biol **13:** 853-859

Finkel T (2006) Intracellular redox regulation by the family of small GTPases. Antioxid Redox Signal **8:** 1857-1863

Franklin KA, Quail PH (2010) Phytochrome functions in Arabidopsis development. J Exp Bot **61:** 11-24

Fu Y, Gu Y, Zheng Z, Wasteneys G, Yang Z (2005) Arabidopsis interdigitating cell growth requires two antagonistic pathways with opposing action on cell morphogenesis. Cell **120:** 687-700

Fu Y, Xu T, Zhu L, Wen M, Yang Z (2009) A ROP GTPase signaling pathway controls cortical microtubule ordering and cell expansion in Arabidopsis. Curr Biol **19:** 1827-1832

Fukushima A, Kusano M, Nakamichi N, Kobayashi M, Hayashi N, Sakakibara H, Mizuno T, Saito K (2009) Impact of clock-associated Arabidopsis pseudo-response regulators in metabolic coordination. Proc Natl Acad Sci U S A **106:** 7251-7256

Gendreau E, Hofte H, Grandjean O, Brown S, Traas J (1998) Phytochrome controls the number of endoreduplication cycles in the Arabidopsis thaliana hypocotyl. Plant J **13:** 221-230

Guimil S, Dunand C (2007) Cell growth and differentiation in Arabidopsis epidermal cells. J Exp Bot **58:** 3829-3840

Huang W, Pérez-García P, Pokhilko A, Millar AJ, Antoshechkin I, Riechmann JL, Mas P (2012) Mapping the core of the Arabidopsis circadian clock defines the network structure of the oscillator. Science **336**:75-79

Kant P, Gordon M, Kant S, Zolla G, Davydov O, Heimer YM, Chalifa-Caspi V, Shaked R, Barak S (2008) Functional-genomics-based identification of genes that regulate Arabidopsis responses to multiple abiotic stresses. Plant Cell Environ **31:** 697-714

Kevei E, Gyula P, Feher B, Toth R, Viczian A, Kircher S, Rea D, Dorjgotov D, Schafer E, Millar AJ, Kozma-Bognar L, Nagy F (2007) Arabidopsis thaliana circadian clock is regulated by the small GTPase LIP1. Current Biology **17:** 1456-1464

Kevei E, Gyula P, Hall A, Kozma-Bognar L, Kim WY, Eriksson ME, Toth R, Hanano S, Feher B, Southern MM, Bastow RM, Viczian A, Hibberd V, Davis SJ, Somers DE, Nagy F, Millar AJ (2006) Forward genetic analysis of the circadian clock separates the multiple functions of ZEITLUPE. Plant Physiol **140:** 933-945

Lammens T, Boudolf V, Kheibarshekan L, Zalmas LP, Gaamouche T, Maes S, Vanstraelen M, Kondorosi E, La Thangue NB, Govaerts W, Inze D, De Veylder L (2008) Atypical E2F activity restrains APC/CCCS52A2 function obligatory for endocycle onset. Proc Natl Acad Sci U S A **105:** 14721-14726

Legnaioli T, Cuevas J, Mas P (2009) TOC1 functions as a molecular switch connecting the circadian clock with plant responses to drought. EMBO J **28:** 3745-3757

Mas P (2008) Circadian clock function in Arabidopsis thaliana: time beyond transcription. Trends Cell Biol **18:** 273-281

Mockler TC, Guo H, Yang H, Duong H, Lin C (1999) Antagonistic actions of Arabidopsis cryptochromes and phytochrome B in the regulation of floral induction. Development **126:** 2073-2082

Nakamichi N, Kusano M, Fukushima A, Kita M, Ito S, Yamashino T, Saito K, Sakakibara H, Mizuno T (2009) Transcript profiling of an Arabidopsis PSEUDO RESPONSE REGULATOR arrhythmic triple mutant reveals a role for the circadian clock in cold stress response. Plant Cell Physiol **50:** 447-462

Ono E, Wong HL, Kawasaki T, Hasegawa M, Kodama O, Shimamoto K (2001) Essential role of the small GTPase Rac in disease resistance of rice. Proc Natl Acad Sci U S A **98:** 759-764

Palagyi A, Terecskei K, Adam E, Kevei E, Kircher S, Merai Z, Schafer E, Nagy F, Kozma-Bognar L (2010) Functional analysis of amino-terminal domains of the photoreceptor phytochrome B. Plant Physiol **153:** 1834-1845

Park J, Gu Y, Lee Y, Yang Z (2004) Phosphatidic acid induces leaf cell death in Arabidopsis by activating the Rho-related small G protein GTPase-mediated pathway of reactive oxygen species generation. Plant Physiol **134:** 129-136

Pruneda-Paz JL, Kay SA (2010) An expanding universe of circadian networks in higher plants. Trends Plant Sci **15**:259-265

Reed JW, Chory J (1994) Mutational analyses of light-controlled seedling development in Arabidopsis. Semin Cell Biol **5:** 327-334

Reed JW, Nagpal P, Poole DS, Furuya M, Chory J (1993) Mutations in the gene for the red/far-red light receptor phytochrome B alter cell elongation and physiological responses throughout Arabidopsis development. Plant Cell **5:** 147-157

Rizzini L, Favory JJ, Cloix C, Faggionato D, O'Hara A, Kaiserli E, Baumeister R, Schafer E, Nagy F, Jenkins GI, Ulm R (2011) Perception of UV-B by the Arabidopsis UVR8 protein. Science **332:** 103-106

Sanchez A, Shin J, Davis SJ (2011) Abiotic stress and the plant circadian clock. Plant Signal Behav **6:** 223-231

Shin DH, Cho MH, Kim TL, Yoo J, Kim JI, Han YJ, Song PS, Jeon JS, Bhoo SH, Hahn TR (2010) A small GTPase activator protein interacts with cytoplasmic phytochromes in regulating root development. J Biol Chem **285:** 32151-32159

Verkest A, Manes CL, Vercruysse S, Maes S, Van Der Schueren E, Beeckman T, Genschik P, Kuiper M, Inzé D, De Veylder L (2005) The cyclin-dependent kinase inhibitor KRP2 controls the onset of the endoreduplication cycle during Arabidopsis leaf development through inhibition of mitotic CDKA;1 kinase complexes. Plant Cell **17:** 1723-1736

Wang L, Fujiwara S, Somers DE (2010) PRR5 regulates phosphorylation, nuclear import and subnuclear localization of TOC1 in the Arabidopsis circadian clock. EMBO J **29:** 1903-1915

Wong HL, Pinontoan R, Hayashi K, Tabata R, Yaeno T, Hasegawa K, Kojima C, Yoshioka H, Iba K, Kawasaki T, Shimamoto K (2007) Regulation of rice NADPH oxidase by binding of Rac GTPase to its N-terminal extension. Plant Cell **19:** 4022-4034

Yamaguchi-Shinozaki K, Shinozaki K (2006) Transcriptional regulatory networks in cellular responses and tolerance to dehydration and cold stresses. Annu Rev Plant Biol **57:** 781-803

FIGURE LEGENDS

Figure 1. LIP1 regulates cell morphology in a developmental stage-specific manner.

A, Pavement cell morphology in cotyledons of Col-0, *lip1-2*, C24 and *lip1-1* plants grown in 12 h white light / 12 h dark (12:12 LD) cycles for 7 days. Scale bars: 50 µm.

B, Cell Shape Factor values calculated from the area and the perimeter of cotyledon pavement cells. n = 43-54, *t*-test: $P < 0.001$ for both samples. Error bars represent SE.

C, Scanning electron microscope (SEM) images of cotyledons of Col-0, *lip1-2*, C24 and *lip1-1* plants grown in 12:12 LD cycles for 7 days. Scale bars: 200 µm.

D, Close-up of collapsed epidermal cell layer in the cotyledon of *lip1-2* seedlings grown in 12:12 LD cycles for 7 days. Arrows point at collapsed stomata guard cells. SEM image, scale bar: 20µm.

E, SEM images of the first leaves of Col-0 and *lip1-2* plants grown in 12:12 LD cycles for 21 days. Scale bars: 50 µm.

Figure 2. Increased ploidy levels in *lip1* mutants.

Ploidy levels were determined in different parts of 7-day-old wild-type and *lip1* mutant seedlings: cotyledons (A-B), hypocotyls (C) or whole seedlings (D) were used. Alternatively, ploidy levels were determined in the first leaves of 21-day-old Col-0 and *lip1-2* plants (E). Plants were grown in 12:12 LD cycles. Relative ratios of nuclei with the indicated DNA content are plotted. n = 4, one sample contained 10 cotyledons (A-B), 10 hypocotyls (C) , 5 seedlings (D) or 4 leaves (E). Asterisks indicate significant difference from the wild type, as determined by Student's *t*-test: * $P < 0.05$, ** $P < 0.01$, *** $P < 0.001$. Error bars represent SD.

Figure 3. The effect of LIP1 on ploidy levels is light-dependent.

C24 and *lip1-1* (A, C, E) or Col-0 and *lip1-2* (B, D, F) plants were grown in darkness (A, B), in 12:12 LD cycles (C, D) or in continuous white light (E, F) for 6 days. Whole seedlings were used for ploidy level determinations. Data were obtained and analyzed as for Fig. 2. n = 4, asterisks indicate significant difference from the wild type, as determined by Student's *t*-test: * $P < 0.05$, ** $P < 0.01$, *** $P < 0.001$. Error bars represent SD.

Figure 4. LIP1 attenuates endoreplication in red and blue, but not in far-red light.

A-E, Plants of the indicated genotypes were grown in darkness (A, C), in continuous red light (40 µmol m-2 s-1) (B), blue light (40 µmol m-2 s-1) (D), or far-red light (5 µmol m-2 s-1) (E) for 7 days. Whole seedlings were subjected to ploidy level determinations. Data were obtained and analyzed as for Fig. 2. n = 3-5, results of statistical analysis (one way ANOVA, Tukey test) are shown in Figures S3 and S4. Error bars represent SD. Ploidy levels in dark-grown *phyA-211* or *lip1-2 phyA-211* plants were not different from those in Col-0 or *lip1-2* plants (data not shown).

F, Plants were grown in conditions identical to those of for panels A and B. Expression levels of *DEL1* were determined by qRT-PCR assays. Values were normalized to *TUB2/3* mRNA levels. Averages of three independent experiments are shown. Error bars represent SE. Results of *t*-tests indicated that differences between the wild type and any mutant combinations under a given light condition (dark or red light) are not significant ($P > 0.1$ for any combinations).

Figure 5. Physiological responses to light and salt stress are altered in *lip1* mutants.

A-C, Plants were grown in continuous red (A), blue (B), or far-red (C) light at the indicated fluence rates for 4 days, then hypocotyl length of the seedlings was measured. Values were normalized to the hypocotyl length of the corresponding dark-grown seedlings. X axes are logarithmic scale. Error bars represent SE, n = 28-32. Results of statistical tests (one way ANOVA, Tukey test) for panels A-C are shown in Figure S5.

D-E, Col-0 and *lip1-2* mutant seeds were grown in 12:12 LD cycles or continuous darkness (dark) on media with or without 200 mM NaCl. The number of seedlings with emerged radicles were counted daily and expressed as the percentage of the total number of seeds. Error bars represent SE, n = 105-125.

F, Col-0, *lip1-2*, C24 and *lip1-1* seedlings were grown in 12:12 LD cycles for 7 days and transferred to vertical plates with media supplemented with different concentrations of NaCl, as indicated. Root lengths were measured 7 days after the transfer. Values normalized to the root length of plants grown on salt-free media are shown. Error bars represent SE, n = 17-20.

For panels D-F, asterisks indicate significant difference from the wild type, as determined by Student's *t*-test: * $P < 0.05$, ** $P < 0.01$, *** $P < 0.001$.

Figure 6. Complementation of ploidy and salt stress phenotypes of *lip1-2* by LIP1 fusion proteins.

A, Ploidy levels in Col-0, *lip1-2* mutant and *lip1-2* mutants expressing YFP-LIP1, YFP-LIP1-NLS or YFP-LIP1-NES fusion proteins. Plants were grown in continuous white light (80 µmol m^{-2} s^{-1}) for 7 days. n = 4, asterisks indicate significant difference from the wild type, as determined by Student's *t*-test: * $P < 0.05$, ** $P < 0.01$, *** $P < 0.001$. Error bars represent SD.

B, Seedlings expressing YFP-LIP1, YFP-LIP1-NLS or YFP-LIP1-NES fusion proteins in the *lip1-2* mutant background along with Col-0 and *lip1-2* controls were grown in 12:12 LD cycles for 14 days on media with or without 100mM NaCl.

Figure 7. Complementation of photomorphogenic and circadian phenotypes of *lip1-2* by LIP1 fusion proteins.

A-C, Fluence rate curves of hypocotyl elongation in continuous red (A), blue (B) or far-red (C) light. Col-0 (filled squares), *lip1-2* (filled triangles) and seedlings expressing YFP-LIP1 (open circles), YFP-LIP1-NLS (open diamonds) or YFP-LIP1-NES (open triangles) fusion proteins in the *lip1-2* background were grown in constant monochromatic light at the indicated fluence rates for 4 days, then hypocotyl length of the seedlings was measured. Values were normalized to the hypocotyl length of the corresponding dark-grown seedlings. X axes are logarithmic scale. n = 28-32, error bars represent SE. Irrespective of the light conditions, no significant differences were detected between the wild type and either of the transgenic lines (one way ANOVA, Tukey test). Hence, asterisks indicate significant differences between *lip1-2* and the wild type, as determined by Student's *t*-test: * $P < 0.05$, ** $P < 0.01$, *** $P < 0.001$.

D-F, Col-0 (filled squares), *lip1-2* mutants (filled triangles) and *lip1-2* mutants expressing YFP-LIP1 (open circles) (D), YFP-LIP1-NLS (open diamonds) (E) or YFP-LIP1-NES (open triangles) (F) fusion proteins were grown in 12:12 LD cycles for 7 days and transferred to continuous red light at 3 µmol m^{-2} s^{-1} fluence rate. Rhythmic

luminescence of the *CAB2:LUC* marker was measured and values normalized to the mean were plotted. Three independent transgenic lines were measured for each construct with similar results. Representative graphs are shown.

Figure S1. Non-continuous cell layer in the epidermis of cotyledons in *lip1-2* mutants.

A, Bright field and chlorophyll auto-fluorescence images of cotyledon of 7-day old Col-0 and *lip1-2* seedlings grown in 12:12 LD cycles for 7 days. Scale bar: 50 µm.

In the cotyledons, chlorophyll fluorescence is produced by mesophyll and guard cells only, since pavement cells do not contain chloroplasts. In the wild-type sample, fluorescent spots mark chloroplasts in guard cells, whereas in the *lip1-2* mutant the dark patches on the fluorescent background correspond to islands of pavement cells.

B, 30 min FM4-64 membrane dye staining and chlorophyll auto-fluorescence imaged together in the cotyledon of 7-day-old *lip1-2* seedlings grown in 12:12 LD cycles. Z-stack of 12 µm depth (interval: 0.74 µm). Scale bar: 50 µm. Patches of pavement cells with clear red outline (FM4-64 labeled membrane) and without chloroplasts are visible among the chloroplast containing palisade mesophyll cells.

Figure S2. Pavement cell morphology in etiolated plants.

Differential interference images showing pavement cells from the adaxial surface of cotyledons of C24 wild-type and lip1-1 mutant plants grown in darkness for 7 days. Scale bars: 25 µm.

Figure S3. Statistical analysis of ploidy measurements in darkness and continuous red light.

Data presented in Figure 4A-B were analyzed by one-way ANOVA in conjunction with an all pairwise multiple comparison procedures (Tukey's honest significance test) to compare the ratio of nuclei with different DNA content in the indicated genotypes in all possible combinations. Color codes indicate the direction and significance level of changes in the ratio of nuclei with specified DNA content. White color indicates no significant difference between the two compared values ($p>0.05$).

A, Heatmap of statistic data from plants grown in darkness for 7 days.

B, Heatmap of statistic data from plants grown in continuous red light (40 μmol m^{-2} s^{-1}) for 7 days. The *lip1-2 phyB-9* double mutant is most similar to the *phyB-9* single mutant, since there is the least significant difference between these two genotypes.

Figure S4. Statistical analysis of ploidy measurements in darkness and continuous blue light.

Data presented in Figure 4C-D were analyzed by one-way ANOVA in conjunction with an all pairwise multiple comparison procedures (Tukey's honest significance test) to compare the ratio of nuclei with different DNA content in the indicated genotypes in all possible combinations. Color codes indicate the direction and significance level of changes in the ratio of nuclei with specified DNA content. White color indicates no significant difference between the two compared values ($p>0.05$).

A, Heatmap of statistic data from plants grown in darkness for 7 days.

B, Heatmap of statistic data from plants grown in continuous blue light (40 μmol m-2 s-1) for 7 days.

Figure S5. Statistical analysis of hypocotyl measurements in continuous red, blue and far-red light.

Data presented in Figure 5A-C were analyzed by one-way ANOVA in conjunction with an all pair wise multiple comparison procedure (Tukey's honest significance test) to compare the hypocotyl length of the genotypes in all possible combinations. Color codes indicate the direction and significance level of changes in hypocotyl length. White color indicates no significant difference between the two compared values ($P>0.05$). Fluence rate of the particular monochromatic light is indicated on the left side of the panels.

A, Heatmap of statistic data from plants grown in continuous red light.

B, Heatmap of statistic data from plants grown in continuous blue light.

C, Heatmap of statistic data from plants grown in continuous far-red light.

Figure S6. Absolute hypocotyl length data for Figure 5A-C.

A-C, Plants were grown in continuous red (A), blue (B), or far-red (C) light at the indicated fluence rates for 4 days, then hypocotyl length of the seedlings was measured. Dark values (dark) show hypocotyl length of etiolated plants. X axes are logarithmic scale. Error bars represent SE, n = 28-32.

Figure S7. *lip1* mutant plants are hypersensitive to salt.

Seedlings were grown in 12:12 LD cycles for 14 days on media containing different concentrations of salt, as indicated.

Figure S8. The effect of LIP1 on salt stress-induced gene expression.

7-days-old wild-type and *lip1-2* mutant plants grown in 12:12 LD cycles were transferred to media supplemented with 200 mM NaCl at Time =0. Samples were harvested at the times indicated. Expression of *RD29A* (A), *RD29B* (B), *RAB18* (C) and *SOS2* (D) was determined by qRT-PCR assays. Values normalized to *TUB2/3* levels are shown. Averages of two independent measurements are shown. Error bars represent SE.

Figure S9. Manipulation of subcellular localization of YFP-LIP1 fusion proteins.

A, Schematic illustration of the LIP1 fusion constructs. YFP: yellow fluorescent protein; NLS: SV-40 nuclear localization signal; NES: nuclear export signal. Expression of all constructs was driven by the 35S promoter from CaMV.

B, Western-blot analysis of LIP1 protein levels. Non-transformed Col-0 seedlings (1), Col-0 plants expressing YFP from the 35S promoter (2) or *lip1-2* seedlings expressing YFP-LIP1 (3), YFP-LIP1-NLS (4), or YFP-LIP1-NES (5) fusion proteins were grown in continuous white light for 4 days before collecting samples for protein extraction. Two identical gels were blotted and probed separately with antibodies specific to GFP (αGFP) or actin (αACT) in order to detect YFP tags or the constitutively expressed actin proteins, respectively. Protein size markers correspond to the blot showing YFP and YFP fusion proteins.

C, Subcellular localisation of YFP-LIP1 fusion proteins. Epifluorescence images of epidermal hypocotyl cells of transgenic *lip1-2* seedlings expressing YFP-LIP1, YFP-

LIP1-NLS or YFP-LIP1-NES fusion proteins are shown on the left, whereas the corresponding reference images are presented on the right. Seedlings were grown in 12:12 LD cycles for 10 days prior to microscopy. Scale bars represent 10 μm; nu: nucleus.

Figure S10. Complementation of the cell-shape phenotype of *lip1-1* mutants.

lip1-1 plants expressing the indicated LIP1 fusion proteins were grown in continuous white light for 7 days. Fluorescent images are shown, except for YFP-LIP1-NLS in the bottom row. In case of YFP-LIP1-NLS, fluorescent signals were restricted to the nuclei (overlay of bright field and fluorescent image in the inlet) and did not mark the contour of the cells; therefore bright field image shows the cell shape. Scale bars: 13 μm or 50 μm for images in top or in the bottom row, respectively.

TABLES

		Pavement cells		Palisade cells	
Genotype	Cotyledon size (mm^2)	Number	Size (μm^2)	Number	Size (μm^2)
C24 (WT)	2.082 ± 0.176	561 ± 61	3697 ± 202	1797 ± 253	1165 ± 156
lip1-1	1.568 ± 0.194	528 ± 77	2874 ± 175	1894 ± 310	821 ± 129
P	< 0.001	0.53	< 0.001	0.29	0.0041

Table 1. Quantitative characterization of pavement and palisade mesophyll cells on the adaxial surface of cotyledons of light-grown seedlings.

Wild-type and *lip1-1* seedlings were grown in 12:12 LD cycles for 7 days. Digital images were taken of the whole cotyledon or different areas and focal planes of the adaxial surface. The size of cotyledons (n=12-15) and cells at similar position in the cotyledon (n=16-22 per cotyledon) were measured. The number of pavement and palisade cells was calculated by dividing the total cotyledon area by the average area of the particular cell type. Mean values ± SD are shown. The significance of the difference from the wild type was analyzed by Student's *t*-test, corresponding *P* values are shown.

Genotype	Cotyledon size (mm^2)	Pavement cells		Palisade cells	
		Number	Size (μm^2)	Number	Size (μm^2)
C24 (WT)	0.229 ± 0.039	581 ± 75	394 ± 61	1423 ± 281	161 ± 31
lip1-1	0.207 ± 0.031	549 ± 83	368 ± 69	1321 ± 235	136 ± 27
P	0.09	0.47	0.39	0.18	0.12

Table 2. Quantitative characterization of pavement and palisade mesophyll cells on the adaxial surface of cotyledons of etiolated seedlings

Wild-type and *lip1-1* seedlings were grown in darkness for 7 days. Digital images were taken of the whole cotyledon or different areas and focal planes of the adaxial surface. The size of cotyledons (n=9-11) and cells (n=35-60 per cotyledon) was measured. The number of pavement and palisade cells was calculated by dividing the total cotyledon area by the average area of the particular cell type. Mean values ± SD are shown. The significance of the difference from the wild type was analyzed by Student's *t*-test, corresponding *P* values are shown.

Genotype	Period (h)	± SE	$P^{[Col-0]}$	$P^{[lip1-2]}$
Col-0 (WT)	29.95	0.28	-	< 0.001
lip1-2	27.37	0.77	< 0.001	-
YFP-LIP1 [*lip1-2*]	29.74	0.36	0.76	0.0023
YFP-LIP1-NLS [*lip1-2*]	29.33	0.70	0.22	0.0061
YFP-LIP1-NES [*lip1-2*]	27.42	0.31	< 0.001	0.71

Table 3. Period estimates for *CAB2:LUC* reporters in wild-type, *lip1-2* and different YFP-LIP1 fusion protein expressing plants.

Seedlings were grown under 12:12 LD cycles for 7 days and moved to constant to red light (3 μmol m^{-2} s^{-1}). Rhythm analysis was performed with BRASS. Three independent transgenic lines were analyzed for each complementing construct. 32 individual seedlings were measured for each line. Variance-weighted mean periods and SE are shown. The significance of the difference from the wild type ($P^{[Col-0]}$) or the *lip1-2* mutant ($P^{[lip1-2]}$) was analyzed by Student's *t*-test.

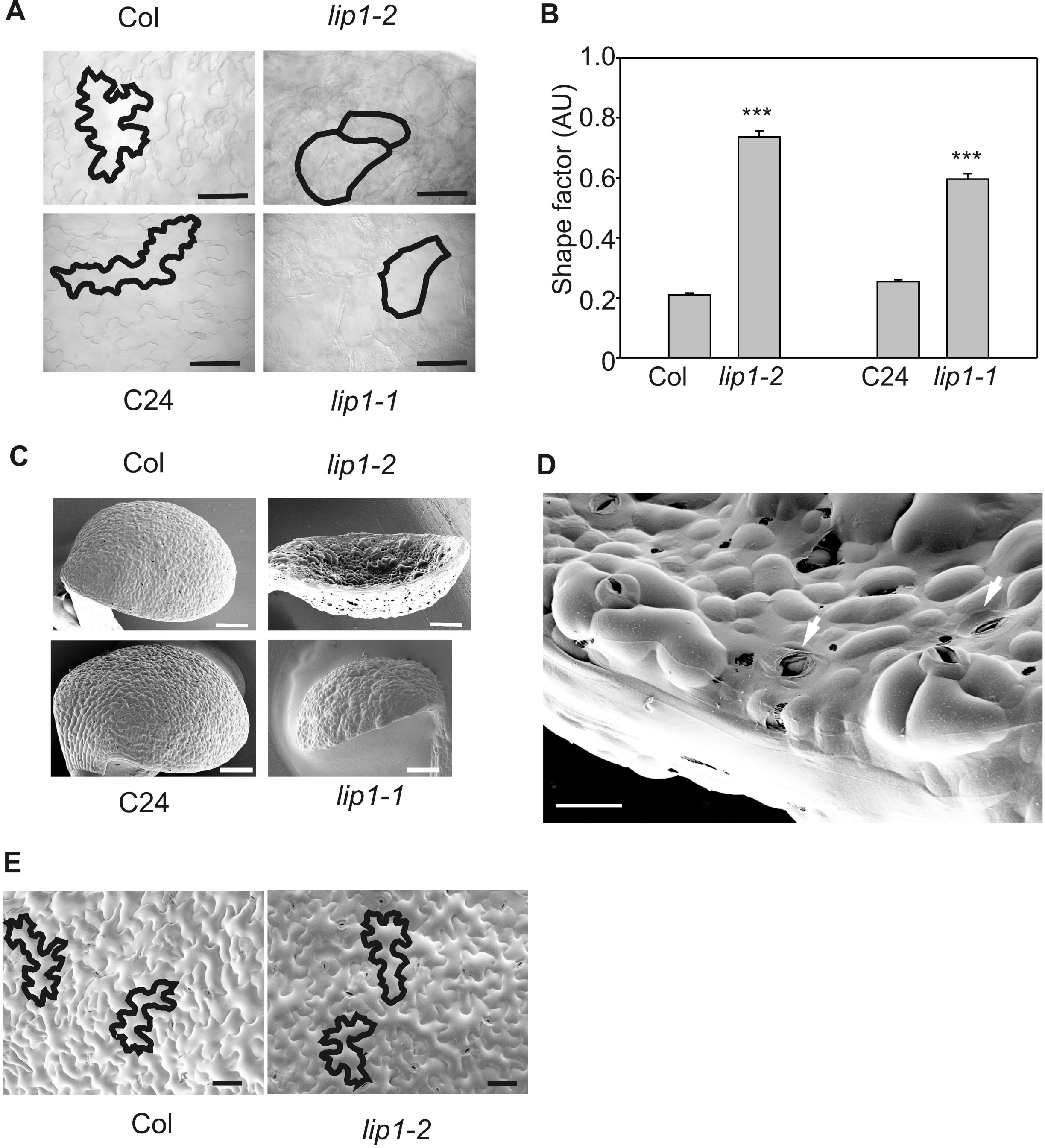

Figure 1. LIP1 regulates cell morphology in a developmental stage-specific manner.
A, Pavement cell morphology in cotyledons of Col-0, *lip1-2*, C24 and *lip1-1* plants grown in 12 h white light / 12 h dark (12:12 LD) cycles for 7 days. Scale bars: 50 µm.
B, Cell Shape Factor values calculated from the area and the perimeter of cotyledon pavement cells. n = 43-54, *t*-test: $P < 0.001$ for both samples. Error bars represent SE.
C, Scanning electron microscope (SEM) images of cotyledons of Col-0, *lip1-2*, C24 and *lip1-1* plants grown in 12:12 LD cycles for 7 days. Scale bars: 200 µm.
D, Close-up of collapsed epidermal cell layer in the cotyledon of *lip1-2* seedlings grown in 12:12 LD cycles for 7 days. Arrows point at collapsed stomata guard cells. SEM image, scale bar: 20µm.
E, SEM images of the first leaves of Col-0 and *lip1-2* plants grown in 12:12 LD cycles for 21 days. Scale bars: 50 µm.

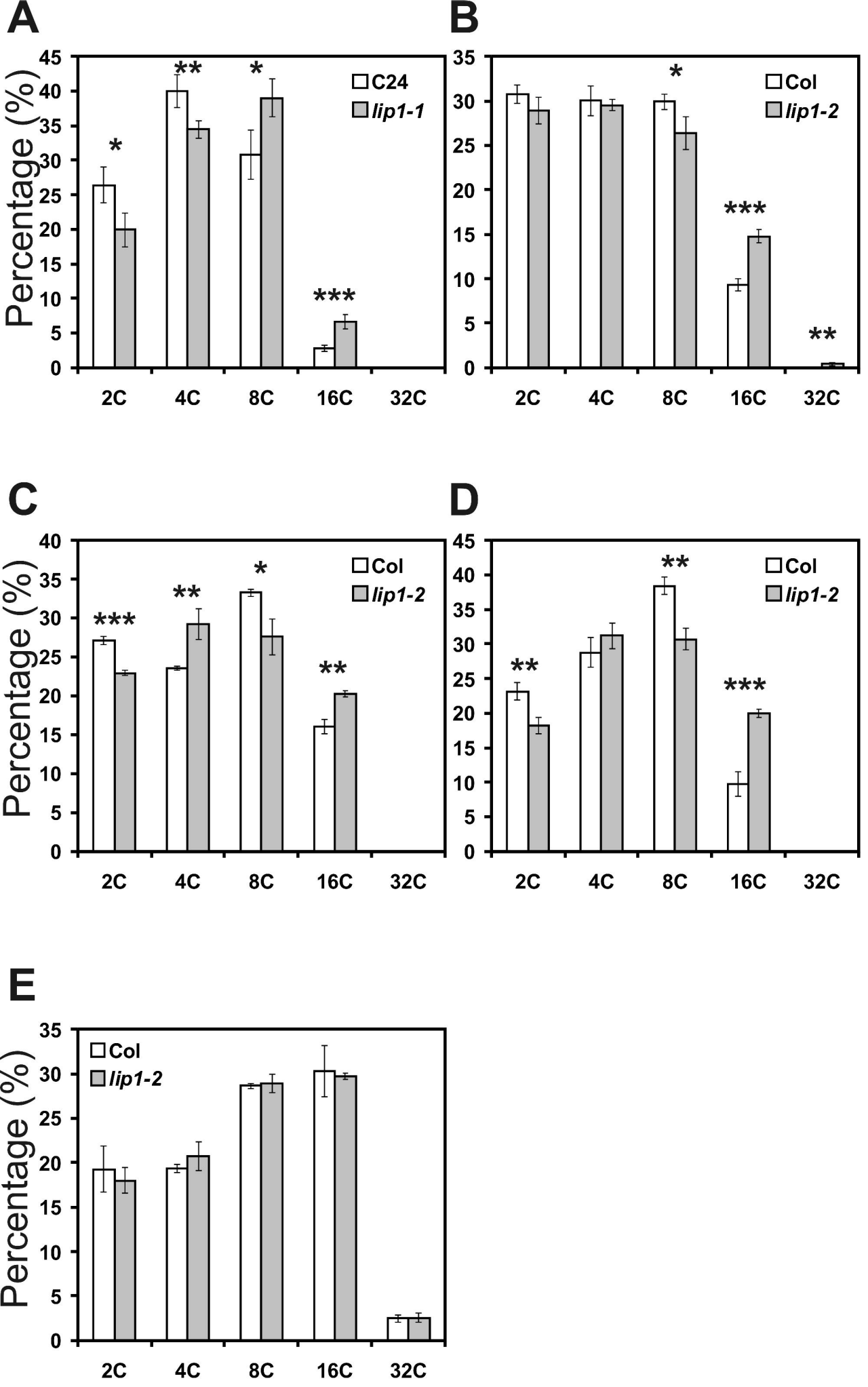

Figure 2. Increased ploidy levels in *lip1* mutants. Ploidy levels were determined in different parts of 7-day-old wild-type and *lip1* mutant seedlings: cotyledons (A-B), hypocotyls (C) or whole seedlings (D) were used. Alternatively, ploidy levels were determined in the first leaves of 21-day-old Col-0 and *lip1-2* plants (E). Plants were grown in 12:12 LD cycles. Relative ratio of nuclei with the indicated DNA content are plotted. n = 4, one sample contained 10 cotyledons (A-B), 10 hypocotyls (C) , 5 seedlings (D) or 4 leaves (E). Asterisks indicate significant difference from the wild type, as determined by Student's *t*-test: * $P < 0.05$, ** $P < 0.01$, *** $P < 0.001$. Error bars represent SD.

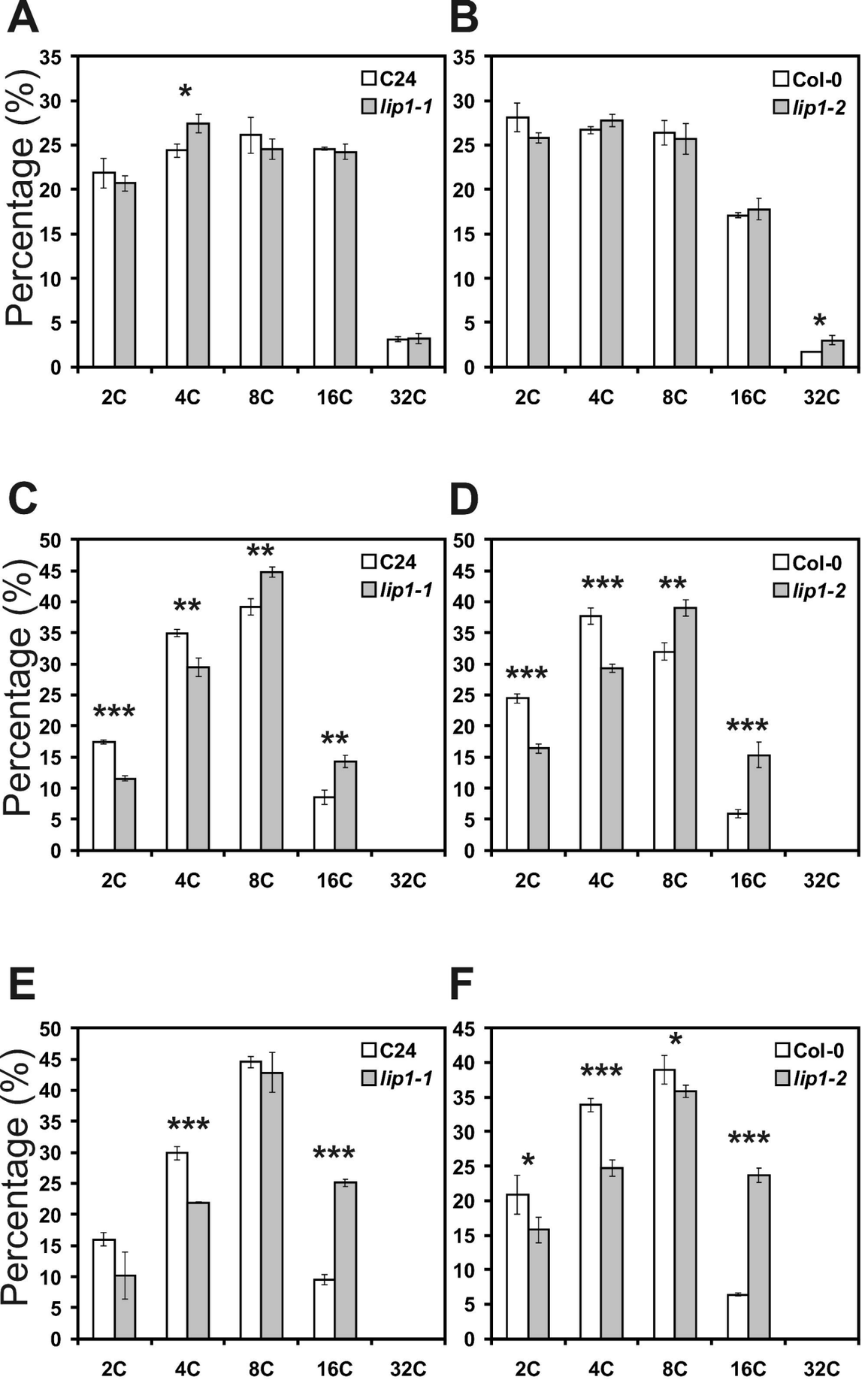

Figure 3. The effect of LIP1 on ploidy levels is light-dependent.

C24 and *lip1-1* (A, C, E) or Col-0 and *lip1-2* (B, D, F) plants were grown in darkness (A, B), in 12:12 LD cycles (C, D) or in continuous white light (E, F) for 6 days. Whole seedlings were used for ploidy level determinations. Data were obtained and analyzed as for Fig. 2. n = 4, asterisks indicate significant difference from the wild type, as determined by Student's *t*-test: * $P < 0.05$, ** $P < 0.01$, *** $P < 0.001$. Error bars represent SD.

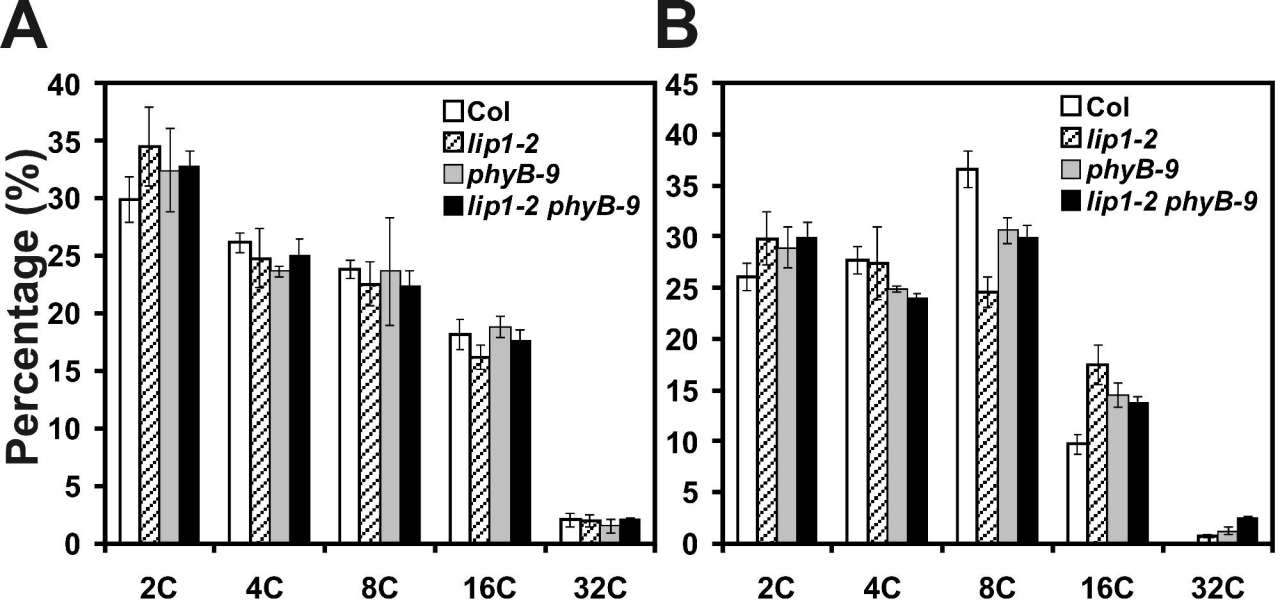

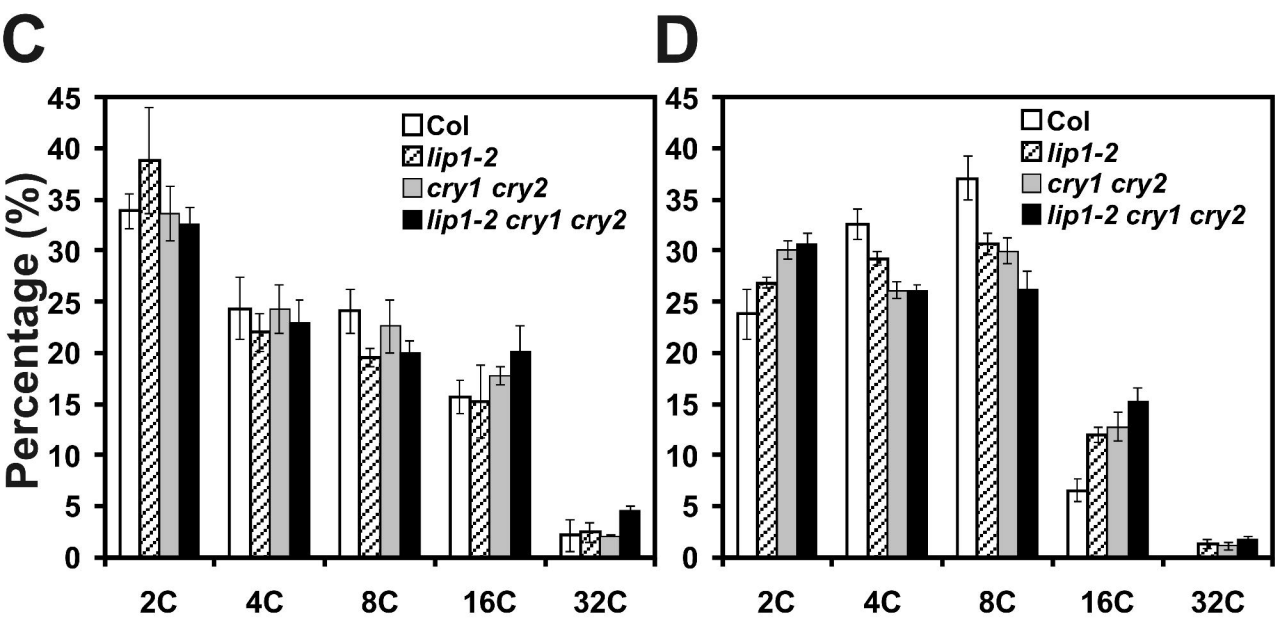

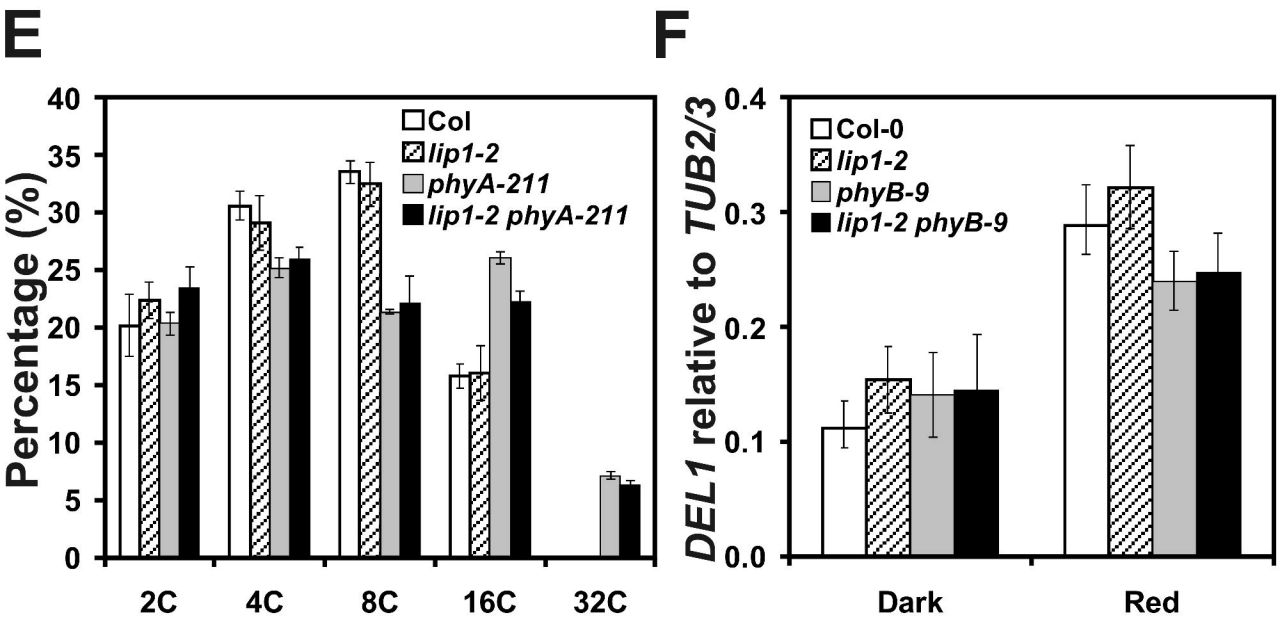

Figure 4. LIP1 attenuates endoreplication in red and blue, but not in far-red light.

A-E, Plants of the indicated genotypes were grown in darkness (A, C), in continuous red light (40 µmol m^{-2} s^{-1}) (B), blue light (40 µmol m^{-2} s^{-1}) (D), or far-red light (5 µmol m^{-2} s^{-1}) (E) for 7 days. Whole seedlings were subjected to ploidy level determinations. Data were obtained and analyzed as for Fig.2. n = 3-5, results of statistical analysis (one way ANOVA, Tukey test) are shown in Figures S2 and S3. Error bars represent SD. Ploidy levels in dark-grown *phyA-211* or *lip1-2 phyA-211* plants were not different from those in Col-0 or *lip1-2* plants (data not shown).

F, Plants were grown in conditions identical to those of for panels A and B. Expression levels of *DEL1* were determined by qRT-PCR assays. Values were normalized to *TUB2/3* mRNA levels. Averages of three independent experiments are shown. Error bars represent SE. Results of *t*-tests indicated that differences between the wild type and any mutant combinations under a given light condition (dark or red light) are not significant ($P > 0.1$ for any combinations).

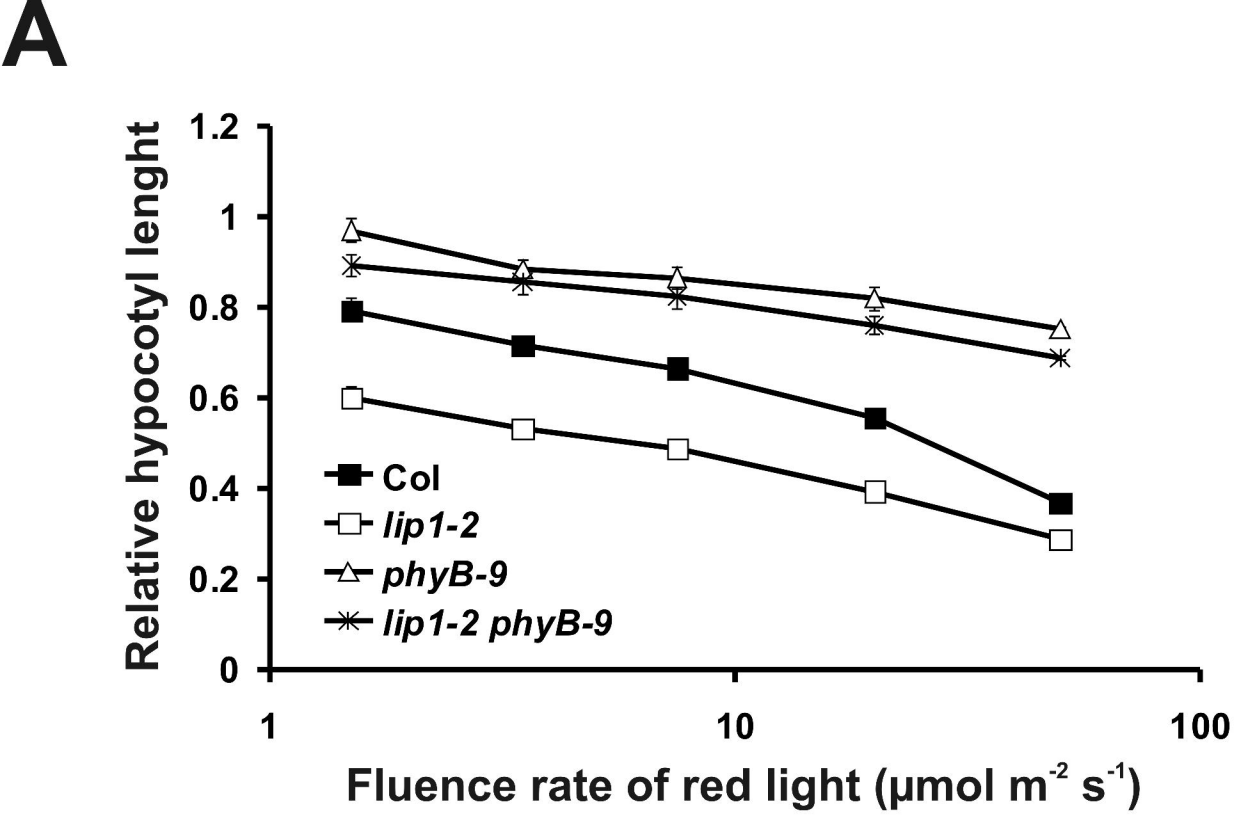

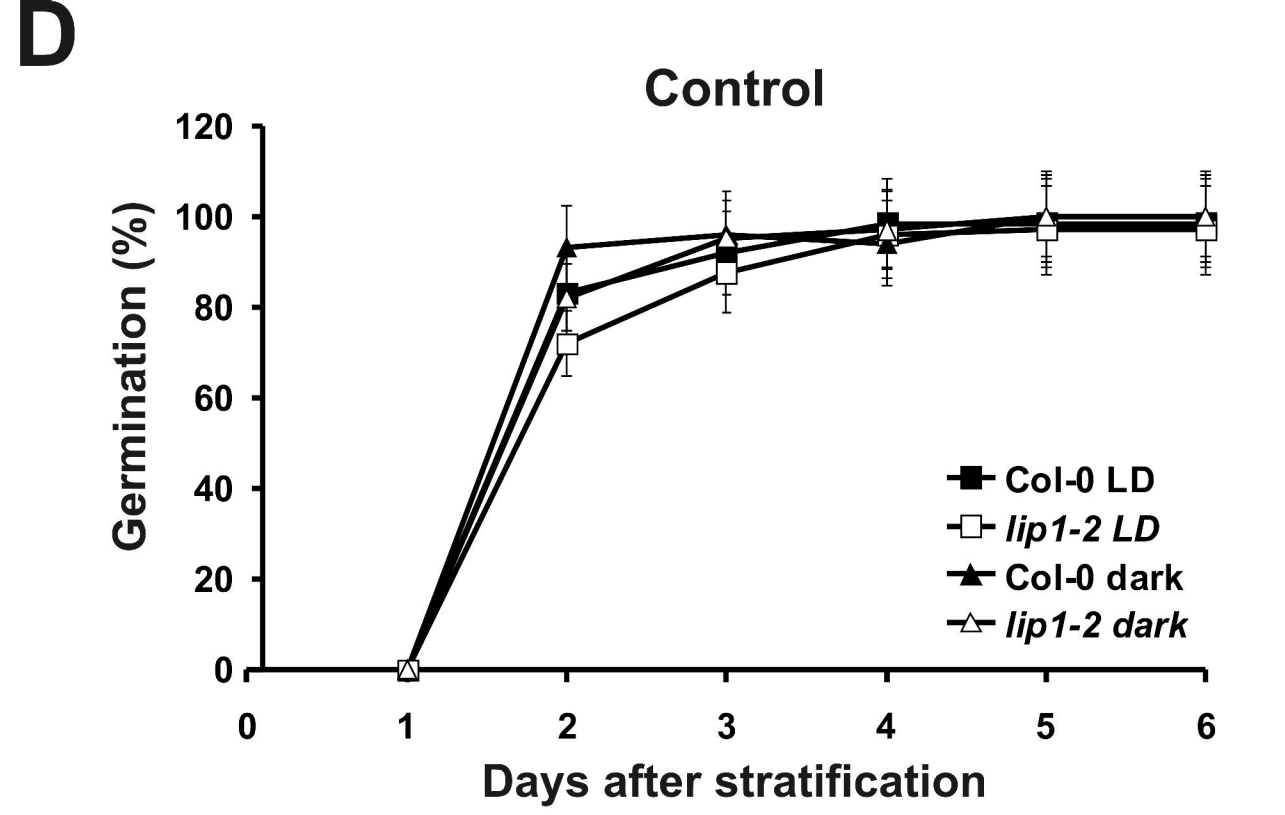

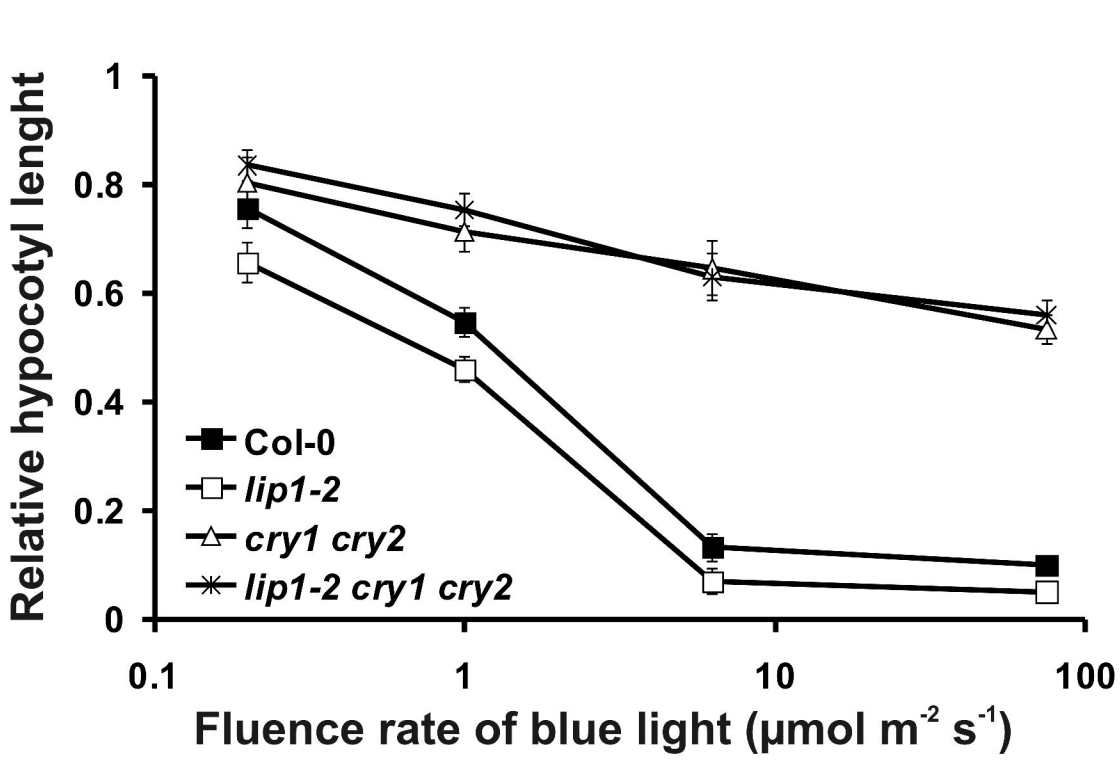

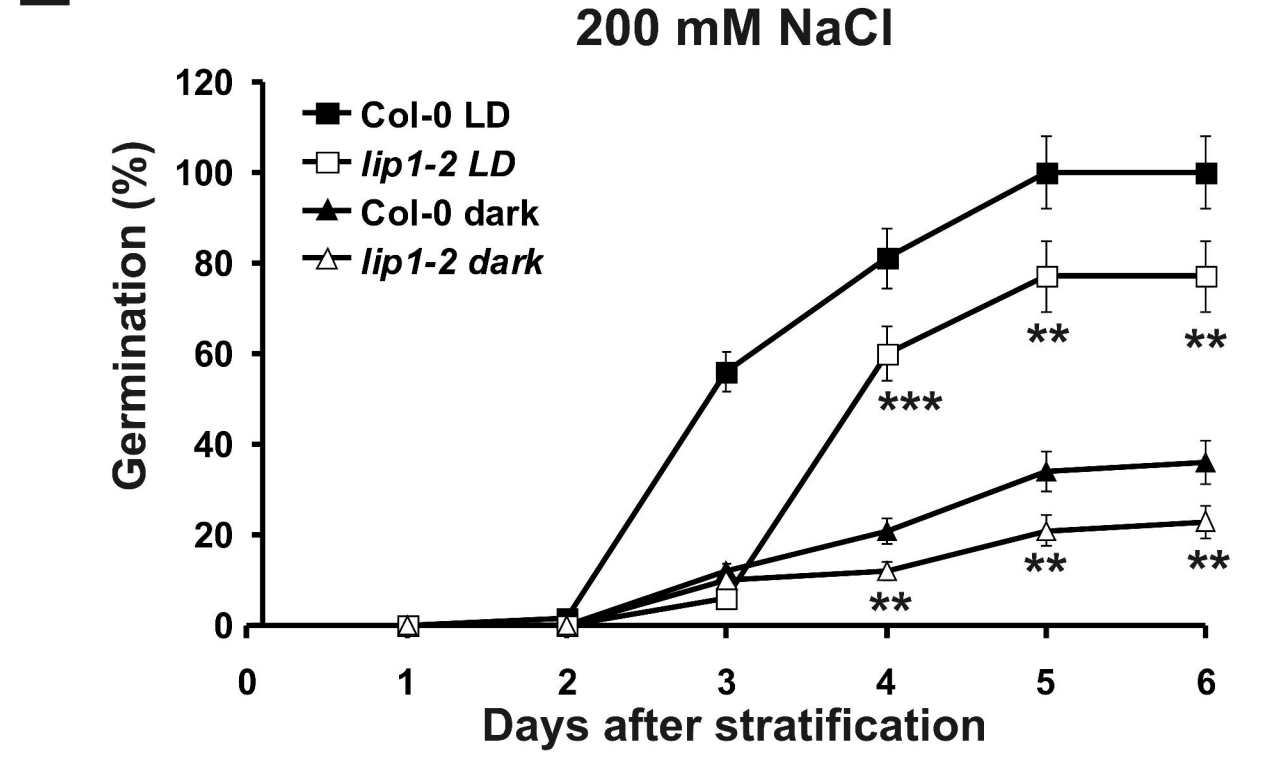

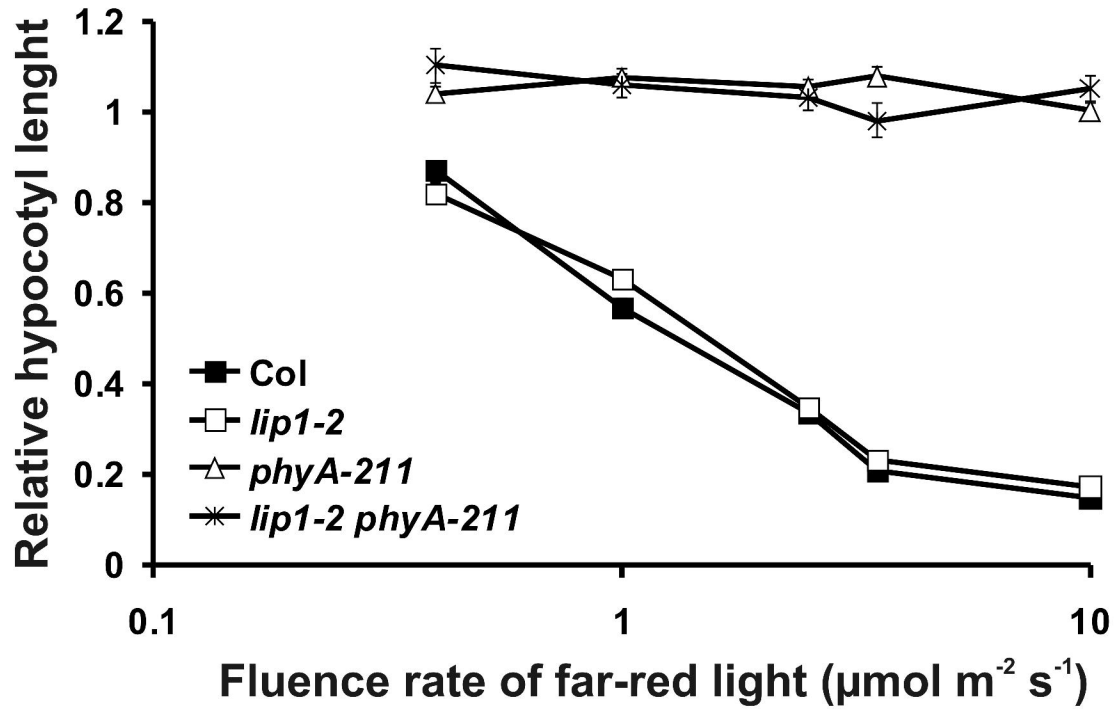

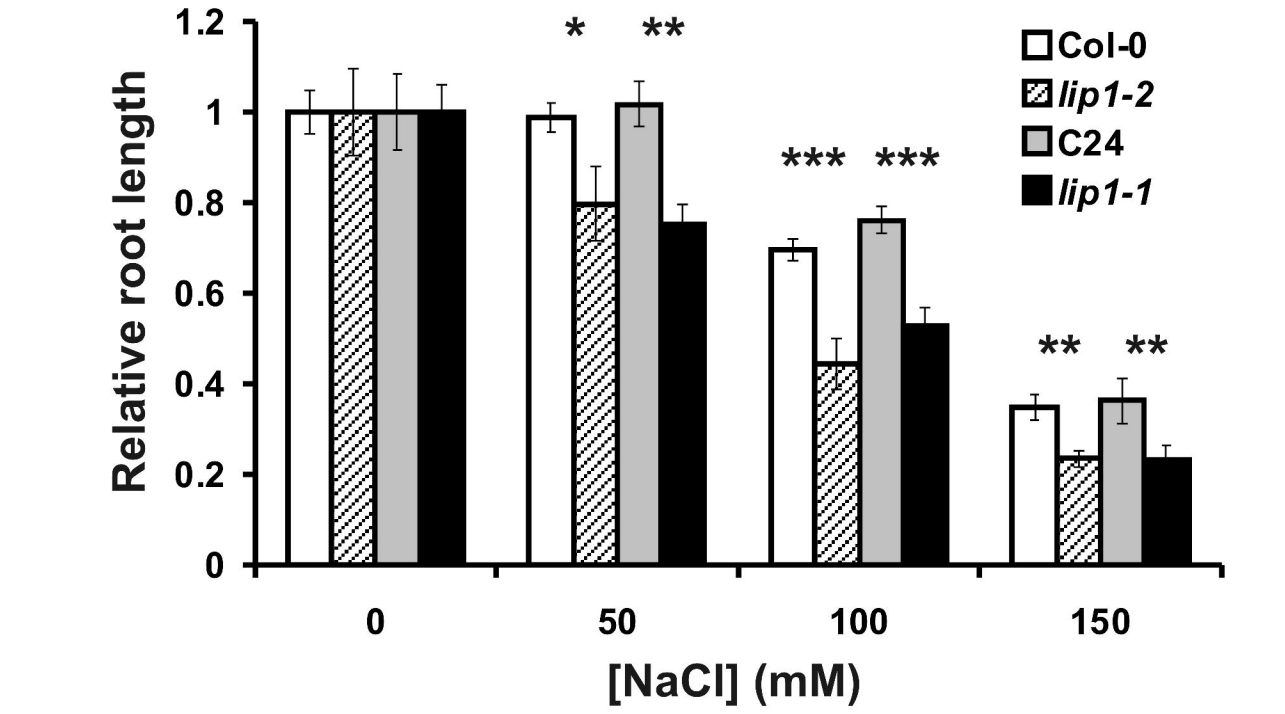

Figure 5. Physiological responses to light and salt stress are altered in *lip1* mutants.

A-C, Plants were grown in continuous red (A), blue (B), or far-red (C) light at the indicated fluence rates for 4 days, then hypocotyl length of the seedlings was measured. Values were normalized to the hypocotyl length of the corresponding dark-grown seedlings. X axes are logarithmic scale. Error bars represent SE, n = 28-32. Results of statistical tests (one way ANOVA, Tukey test) for panels A-C are shown in Figure S5.

D-E, Col-0 and *lip1-2* mutant seeds were grown in 12:12 LD cycles or continuous darkness (dark) at 22°C on media with or without 200 mM NaCl. The number of seedlings with emerged radicles were counted daily and expressed as the percentage of the total number of seeds. Error bars represent SE, n = 105-125.

F, Col-0, *lip1-2*, C24 and *lip1-1* seedlings were grown in 12:12 LD cycles for 7 days and transferred to vertical plates with media supplemented with different concentrations of NaCl, as indicated. Root lengths were measured 7 days after the transfer. Values normalized to the root length of plants grown on salt-free media are shown. Error bars represent SE, n = 17-20.

For panels D-F, asterisks indicate significant difference from the wild type, as determined by Student's *t*-test: * P < 0.05, ** P < 0.01, *** P < 0.001.

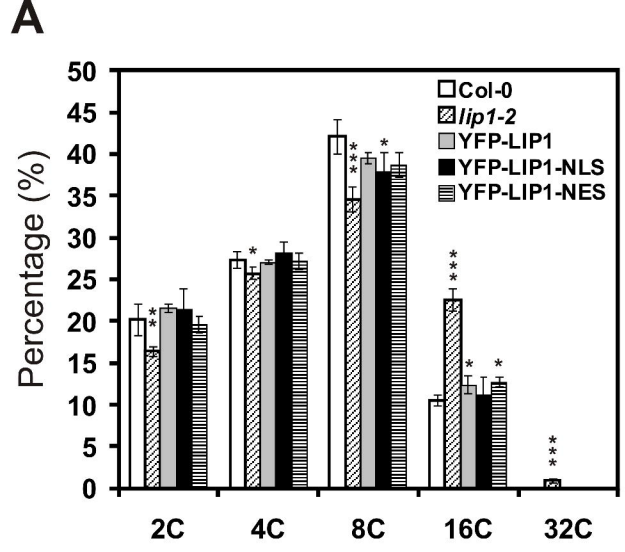

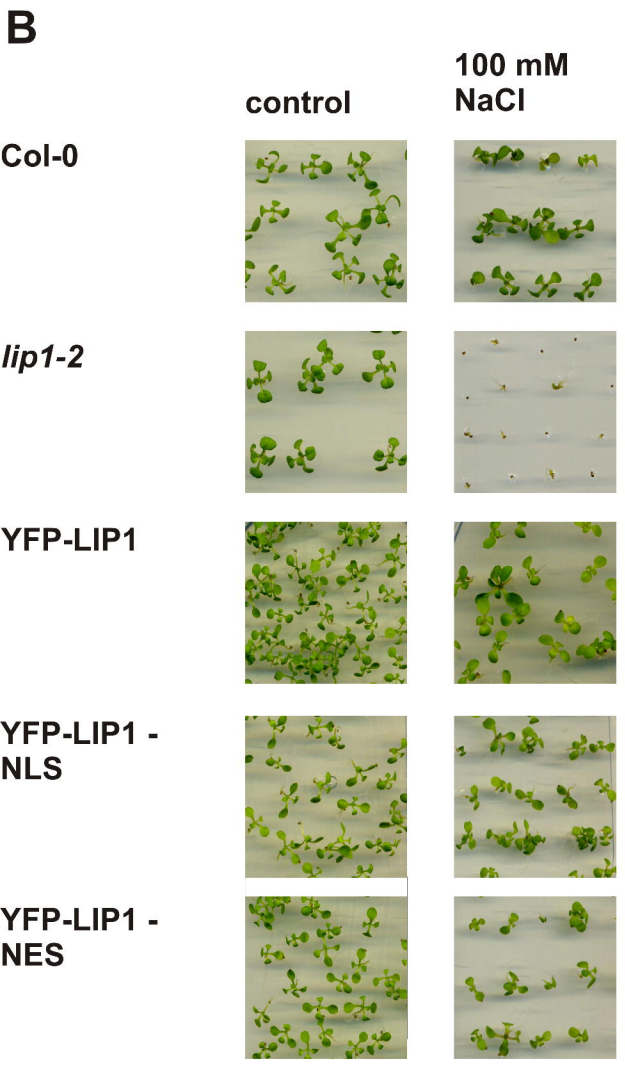

Figure 6. Complementation of ploidy and salt stress phenotypes of *lip1-2* by LIP1 fusion proteins.

A, Ploidy levels in Col-0, *lip1-2* mutant and *lip1-2* mutants expressing YFP-LIP1, YFP-LIP1-NLS or YFP-LIP1-NES fusion proteins. Plants were grown in continuous white light (80 µmol m^{-2} s^{-1}) for 7 days. n = 4, asterisks indicate significant difference from the wild type, as determined by Student's *t*-test: * $P < 0.05$, ** $P < 0.01$, *** $P < 0.001$. Error bars represent SD.

B, Seedlings expressing YFP-LIP1, YFP-LIP1-NLS or YFP-LIP1-NES fusion proteins in the *lip1-2* mutant background along with Col-0 and *lip1-2* controls were grown in 12:12 LD cycles for 14 days on media with or without 100mM NaCl.

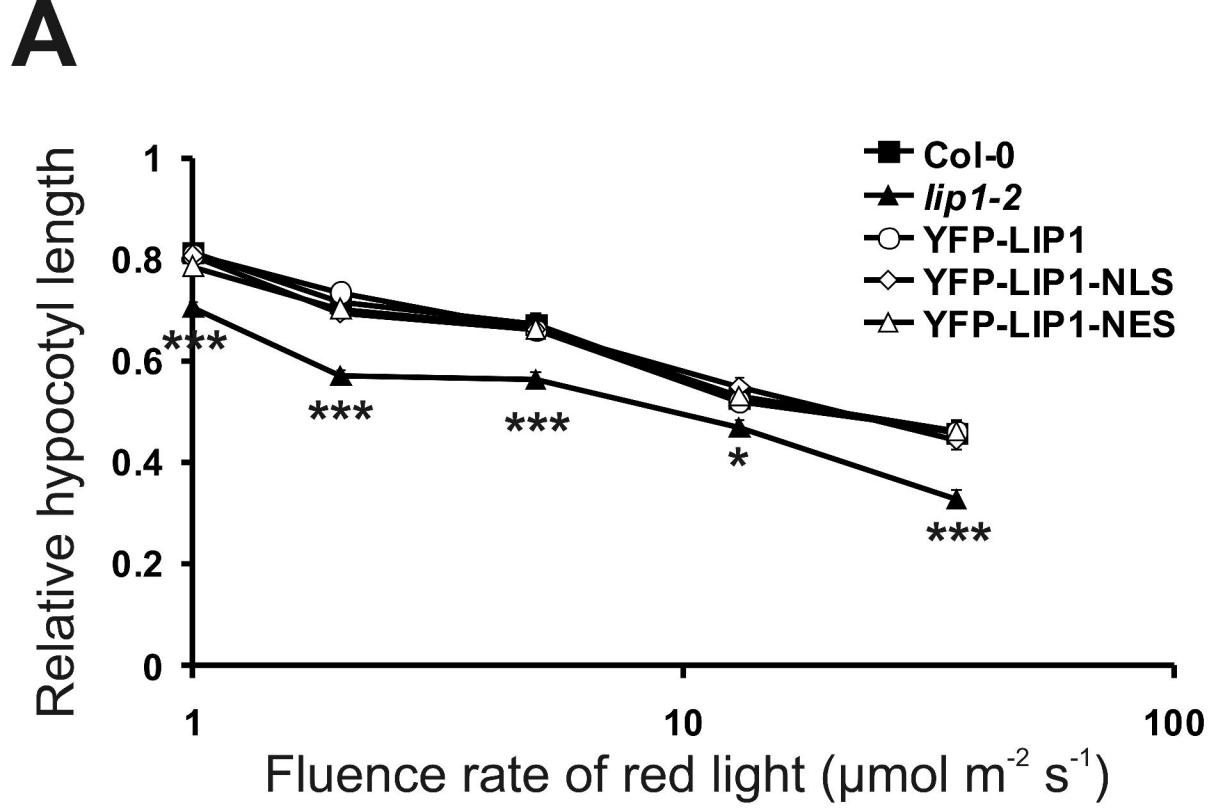

Figure 7. Complementation of photomorphogenic and circadian phenotypes of *lip1-2* by LIP1 fusion proteins.

A-C, Fluence rate curves of hypocotyl elongation in continuous red (A), blue (B) or far-red (C) light. Col-0 (filled squares), *lip1-2* (filled triangles) and seedlings expressing YFP-LIP1 (open circles), YFP-LIP1-NLS (open diamonds) or YFP-LIP1-NES (open triangles) fusion proteins in the *lip1-2* background were grown in constant monochromatic light at the indicated fluence rates for 4 days, then hypocotyl length of the seedlings was measured. Values were normalized to the hypocotyl length of the corresponding dark-grown seedlings. X axes are logarithmic scale. n = 28-32, error bars represent SE. Irrespective of the light conditions, no significant differences were detected between the wild type and either of the transgenic lines (one way ANOVA, Tukey test). Hence, asterisks indicate significant differences between *lip1-2* and the wild type, as determined by Student's t-test: * $P < 0.05$, ** $P < 0.01$, *** $P < 0.001$.
D-F, Col-0 (filled squares), *lip1-2* mutants (filled triangles) and *lip1-2* mutants expressing YFP-LIP1 (open circles) (D), YFP-LIP1-NLS (open diamonds) (E) or YFP-LIP1-NES (open triangles) (F) fusion proteins were grown in 12:12 LD cycles for 7 days and transferred to continuous red light at 3 µmol m^{-2} s^{-1} fluence rate. Rhythmic luminescence of the *CAB2:LUC* marker was measured and values normalized to the mean were plotted. Three independent transgenic lines were measured for each construct with similar results. Representative graphs are shown.